AGU PUBLICATIONS

Global Biogeochemical Cycles

RESEARCH ARTICLE
10.1002/2017GB005633

Key Points:
- Negative nitrogen cycle feedbacks reduce anthropogenic perturbations
- Oceanic N_2O emissions are predicted to decline by 2100
- Anthropogenically driven changes in ocean circulation and atmospheric N deposition combine to intensify OMZs

Supporting Information:
- Supporting Information S1

Correspondence to:
A. Landolfi,
alandolfi@geomar.de

Citation:
Landolfi, A., C. J. Somes, W. Koeve, L. M. Zamora, and A. Oschlies (2017), Oceanic nitrogen cycling and N_2O flux perturbations in the Anthropocene, *Global Biogeochem. Cycles*, *31*, 1236–1255, doi:10.1002/2017GB005633.

Received 30 JAN 2017
Accepted 18 JUL 2017
Accepted article online 24 JUL 2017
Published online 13 AUG 2017

Oceanic nitrogen cycling and N_2O flux perturbations in the Anthropocene

A. Landolfi[1], C. J. Somes[1], W. Koeve[1], L. M. Zamora[2,3], and A. Oschlies[1]

[1]GEOMAR Helmholtz-Zentrum für Ozeanforschung Kiel, Marine Biogeochemical Modelling, Kiel, Germany, [2]Earth System Science Interdisciplinary Center, University of Maryland, College Park, Maryland, USA, [3]NASA Goddard Space Flight Center, Greenbelt, Maryland, USA

Abstract There is currently no consensus on how humans are affecting the marine nitrogen (N) cycle, which limits marine biological production and CO_2 uptake. Anthropogenic changes in ocean warming, deoxygenation, and atmospheric N deposition can all individually affect the marine N cycle and the oceanic production of the greenhouse gas nitrous oxide (N_2O). However, the combined effect of these perturbations on marine N cycling, ocean productivity, and marine N_2O production is poorly understood. Here we use an Earth system model of intermediate complexity to investigate the combined effects of estimated 21st century CO_2 atmospheric forcing and atmospheric N deposition. Our simulations suggest that anthropogenic perturbations cause only a small imbalance to the N cycle relative to preindustrial conditions (~+5 Tg N y^{-1} in 2100). More N loss from water column denitrification in expanded oxygen minimum zones (OMZs) is counteracted by less benthic denitrification, due to the stratification-induced reduction in organic matter export. The larger atmospheric N load is offset by reduced N inputs by marine N_2 fixation. Our model predicts a decline in oceanic N_2O emissions by 2100. This is induced by the decrease in organic matter export and associated N_2O production and by the anthropogenically driven changes in ocean circulation and atmospheric N_2O concentrations. After comprehensively accounting for a series of complex physical-biogeochemical interactions, this study suggests that N flux imbalances are limited by biogeochemical feedbacks that help stabilize the marine N inventory against anthropogenic changes. These findings support the hypothesis that strong negative feedbacks regulate the marine N inventory on centennial time scales.

1. Introduction

Nitrogen (N) is an essential nutrient for the maintenance of marine biological production, and its availability regulates the biological sequestration of CO_2 by marine phytoplankton [*Falkowski*, 1997]. N inputs from biological N_2 fixation, the main oceanic natural source of fixed nitrogen, balance the loss of fixed N, occurring via denitrification and anammox under low-oxygen conditions to maintain a stable oceanic N inventory and ocean productivity [*Gruber*, 2016]. Anthropogenic perturbations directly alter this balance by increasing atmospheric nitrogen inputs [*Duce et al.*, 2008; *Lamarque et al.*, 2013] and indirectly affect N_2 fixation [*Krishnamurthy et al.*, 2007, 2009; *McMahon et al.*, 2015] and N loss by warming and deoxygenating the ocean [*Gruber*, 2016], potentially leading to intensified N_2O production [*Babbin et al.*, 2015]. The effects of these combined anthropogenic perturbations on the marine N cycle are still highly uncertain [*Gruber*, 2016], and the net impact on the production and remineralization of organic matter in the ocean and on the air-sea gas exchange of greenhouse gases such as N_2O remains to be assessed.

Numerous 21st century projections predict that warming-induced changes in physical circulation and mixing will reduce upper ocean nutrient supply, lowering ocean productivity, organic matter export [*Steinacher et al.*, 2010; *Bopp et al.*, 2013], and oceanic N_2O emissions [*Martinez-Rey et al.*, 2015]. Other studies suggest that direct temperature effects on metabolic processes [*Eppley*, 1972] may counteract the decline in nutrient supply leading to increased organic matter production and remineralization [*Matsumoto*, 2007; *Schmittner et al.*, 2008; *Taucher and Oschlies*, 2011; *Segschneider and Bendtsen*, 2013] and possible ecosystem restructuring [*Segschneider and Bendtsen*, 2013; *Dutkiewicz et al.*, 2013]. Marine N_2 fixing organisms with temperature optima above 20°C [*Breitbarth et al.*, 2007; *Moisander et al.*, 2010] are expected to be favored by rising temperatures, potentially enhancing N availability [*McMahon et al.*, 2015]. Others have suggested that changes

Table 1. Studies Addressing N Cycle Perturbations[a]

	Forcings:			Model Processes:	
Study	Warming	N Deposition	Atm N_2O	N Feedbacks	N_2O Cycle
Krishnamurthy et al. [2007]		✓[b]		✓[c]	
Krishnamurthy et al. [2009]		✓		✓[c]	
Krishnamurthy et al. [2010]		✓		✓[c]	
Suntharalingam et al. [2012]		✓			✓
Somes et al. [2016]		✓[b]		✓	
Yang and Gruber [2016]		✓		✓	
Martinez-Rey et al. [2015]	✓		✓[d]		✓
J. K. Moore et al. [2013]	✓	✓		✓[c]	
This study	✓	✓	✓	✓	✓

[a]Forcings (warming, transient atmospheric N deposition, atmospheric N_2O concentrations), N cycle processes and parameterizations of N_2O cycle. Fully prognostic N cycle processes include prognostic water column and benthic denitrification (WCD, BD) and N_2 fixation.
[b]Constant atmospheric N deposition scenario.
[c]Not fully prognostic denitrification.
[d]Constant preindustrial atmospheric N_2O concentration.

in remineralization rates may redistribute nutrients and change marine production [*Kwon et al.*, 2009; *Segschneider and Bendtsen*, 2013; *Yool et al.*, 2013], which may affect deoxygenation and denitrification.

Increases in anthropogenic atmospheric N deposition to the ocean adds further complexity, potentially relieving the widespread N limitation [*C. M. Moore et al.*, 2013], which may stimulate export production [*Suntharalingam et al.*, 2012; *Kim et al.*, 2014] and intensify N_2O production in some regions [*Suntharalingam et al.*, 2012]. Other studies suggest that external N additions may enhance net N loss due to the onset of positive feedbacks [*Landolfi et al.*, 2013] that can reduce the impact of atmospheric deposition on ocean productivity [*Somes et al.*, 2016; *Yang and Gruber*, 2016] and potentially affect N_2O production.

Given the potentially opposing impacts related to ocean warming, deoxygenation, and atmospheric N deposition, and the numerous feedbacks involved in the N cycle, a comprehensive assessment of the sensitivity of the marine N cycle to the combined perturbations is required. Such studies have been hindered by the complexity of the N cycle and the lack of full representation of N cycle feedbacks in models (Table 1), limiting robust projections of the biogeochemical feedbacks under future climate.

Here we use an Earth system model of intermediate complexity, which includes temperature-dependent metabolic processes and fully prognostic N cycle processes, N_2 fixation, water column denitrification (WCD), and benthic denitrification (BD), to assess the individual and, for the first time, combined effects of ocean warming, ocean deoxygenation, and atmospheric N deposition on the oceanic N cycle. Our goal is to disentangle the effects of individual stressors and to quantify their combined net effects on the marine N cycle, ocean productivity, and air-sea N_2O flux.

2. Model Description

The model used here is a modified version from the Kiel 2.9 UVic Earth System Climate Model (Uvic) [*Somes and Oschlies*, 2015], which includes a N_2O parameterization [*Zamora and Oschlies*, 2014]. This model has been extensively used and reproduces the large- scale patterns of physical and biogeochemical ocean tracers well [*Keller et al.*, 2012; *Zamora and Oschlies*, 2014; *Somes and Oschlies*, 2015].

2.1. The Physical Model

The physical ocean-atmosphere-sea ice model includes a three-dimensional (1.8 × 3.6°, 19 vertical levels) general circulation model of the ocean (Modular Ocean Model 2) with parameterizations such as diffusive mixing along and across isopycnals, eddy-induced tracer advection [*Gent and McWilliams*, 1990], computation of tidally induced diapycnal mixing over rough topography [*Simmons et al.*, 2004], and an anisotropic viscosity scheme [*Large et al.*, 2001] to better resolve zonal equatorial currents. Additionally, to account for the unresolved deep zonal equatorial jets that ventilate the suboxic zones [*Dietze and Löeptien*, 2013], an equatorial isopycnal mixing scheme [*Getzlaff and Dietze*, 2013] is included. This improves equatorial circulation

and the representation of global oxygen minimum zones volumes within observational uncertainties [*Bianchi et al.*, 2012], allowing for the simulation of global water column denitrification rates without applying artificial thresholds to reduce denitrification rates [*J. K. Moore et al.*, 2013; *Somes et al.*, 2013]. We use a two-dimensional, single-level energy-moisture balance atmosphere and a dynamic-thermodynamic sea ice model, forced with prescribed monthly climatological winds [*Kalnay et al.*, 1996] and ice sheets [*Peltier*, 2004].

2.2. The Biogeochemical Model

The marine ecosystem-biogeochemical component is based on *Keller et al.* [2012] with modifications from *Somes and Oschlies* [2015] and includes nitrous oxide (N_2O) following *Zamora and Oschlies* [2014]. The state variables include two phytoplankton classes, N_2-fixing diazotrophs (Dia) and ordinary phytoplankton (P), zooplankton (Z), particulate detritus (D), nitrate (NO_3), phosphate (PO_4^{3-}), dissolved oxygen (O_2), dissolved organic nitrogen (DON), dissolved organic phosphorus (DOP), dissolved inorganic carbon (DIC), natural ^{14}C, and N_2O. Prognostic iron (Fe) is not included in our model, but iron limitation for both phytoplankton classes is calculated as in *Keller et al.* [2012] using prescribed modeled monthly mean dissolved iron concentrations [*Galbraith et al.*, 2010]. Our model includes temperature-dependent metabolic rates as suggested both by theoretical [*Gillooly et al.*, 2001] and experimental grounds [*Eppley*, 1972; *Bendtsen et al.*, 2015; *Marsay et al.*, 2015]. Briefly, the maximum potential growth rate of both phytoplankton classes follows the Eppley-type [*Eppley*, 1972] temperature-dependent function: $J_{max}=a\cdot\exp\left(\frac{T}{T_b}\right)\frac{[Fe]}{k_{Fe}+[Fe]}$ and depends on Fe concentrations (see Table S1 in the supporting information for parameter values). The growth rate of nonfixing phytoplankton (P) is then determined by irradiance I, $[NO_3]$, $[PO_4]$, and [DOP]:

$$\bar{J}=J_{max}\min\left[\frac{\alpha I}{\left(J_{max}^2+(\alpha I)^2\right)^{1/2}},\frac{[NO_3]}{k_{NO_3}+[NO_3]},\max\left(\frac{[PO_4]}{k_{PO_4}+[PO_4]},h_{dop}\frac{[DOP]}{k_{DOP}+[DOP]}\right)\right] \quad (1)$$

The *Dia* growth rate is computed similarly, but without a nitrate limitation term. To represent the whole diazotroph community, the temperature dependency used here differs from previous formulations [*Schmittner et al.*, 2008; *Keller et al.*, 2012], allowing for growth at temperatures below 15°C as in *Somes and Oschlies* [2015]. Zooplankton maximum potential growth is reduced where O_2 falls below 7 mmol m^{-3} and is dependent on temperature, T (°C): $g_z^{max}=g_z\cdot\max[0,0.5[\tanh(O_2-8)+1]b^{c_z(20,T)}]$, with O_2 in mmol m^{-3}, (Table S1). Potential growth rate is capped for temperatures above 20°C. This allows to avoid unrealistically high grazing rates in the tropics [*Keller et al.*, 2012]. The remineralization rate of detritus is temperature dependent and decreases by a factor of 5 in oxygen-deficient waters following $\mu_D=\mu_{D0}\cdot\exp\left(\frac{T}{T_b}\right)[0.75+0.25\tanh(O_2-6)]$. The model also includes a temperature-dependent fast remineralization term from phytoplankton, to mimic the fast recycling microbial loop, and temperature-dependent remineralization rate for DON and DOP with the same *e*-folding temperature dependence as for sinking detrital matter (Table S1). Oxygen is consumed in the fast recycling microbial loop and via particulate and dissolved organic matter remineralization assuming a constant O_2:P ratio, 160:1. O_2 consumption is inhibited in O_2-deficient waters ($O_2<7$ mmol m^{-3}) following: $r_{sox}^{O_2}=0.5[\tanh(O_2-3)+1]$ and replaced by oxygen-equivalent oxidation by nitrate following: $r_{sox}^{NO_3}=0.5[1-\tanh(O_2-3)]$. The model includes both benthic denitrification (BD) and water column denitrification (WCD), which implicitly includes anammox. BD parameterization is based on the rain ratio of carbon flux onto the sediments (assuming C:N = 6.625) and bottom water oxygen and nitrate [*Bohlen et al.*, 2012]. Since continental shelves are not well resolved in the model, a subgrid-scale bathymetry parameterization is included [*Somes and Oschlies*, 2015]. The oceanic subsurface N_2O production (J_{N_2O}), here defined as total production, is parameterized following *Zamora and Oschlies* [2014], as a function of O_2 consumption ($J(O_2)_{consumption}$) with a linear O_2 dependency, inherently including both nitrification and denitrification [*Zamora et al.*, 2012]. In O_2-deficient waters (<4 mmol m^{-3}), denitrification becomes a sink of N_2O in our model, that is consumed at a constant rate, c (Table S1). The gradient driving the air-sea N_2O gas exchange, F_{sfc}, is computed online based on departure of the surface ocean concentration from the saturation value using the solubility coefficients of *Weiss and Price* [1980] and time-varying prescribed atmospheric N_2O concentrations (historical and RCP8.5). Lacking an atmospheric chemistry model, we use these atmospheric N_2O concentrations rather than global N_2O emissions to the atmosphere. The N_2O oceanic sources minus sink terms (SMS_{N_2O}) are

$$SMS_{N_2O}=F_{sfc}+J_{N_2O}-c \quad (2)$$

$$J_{N_2O}=\left(b+m[O_2]\right)J(O_2)_{consumption}\qquad Z>Z_{euph.} \quad (3)$$

We take a conservative approach inhibiting N_2O production in surface waters to mimic light inhibition of nitrification [*Ward*, 2013] similar to previous studies [e.g., *Suntharalingam et al.*, 2012; *Zamora and Oschlies*, 2014]. Subsurface N_2O production occurring below the O_2 level of 10 mmol m^{-3} is diagnosed online. In our model, this represents the N_2O production via the "low-O_2 pathway," associated with the combination of denitrification and nitrification. The difference between the total N_2O production and the low-O_2 pathway production is taken to represent "high-O_2 pathway," ascribed to nitrification only. This pragmatic approach, although indicative, is unable to single out the contribution of nitrification and denitrification which can occur also simultaneously [e.g., *Ward*, 2013; *Ji et al.*, 2015]. A rigorous separation of the two processes would require more mechanistic parameterizations that have been hindered by the still large conceptual and parametric uncertainties [*Babbin et al.*, 2015; *Ji et al.*, 2015; *Trimmer et al.*, 2016].

2.3. Model Experiments

We performed four model experiments: (1) WARM to account for the warming-induced effects under increasing atmospheric CO_2 forcing and N_2O concentrations, and constant preindustrial atmospheric N deposition; (2) NDEP to account for effects of the increasing atmospheric N deposition at constant preindustrial CO_2 forcing, N_2O concentrations, and climate; (3) FULL to account for the combined effects of warming and atmospheric N deposition under increasing atmospheric CO_2 forcing, N_2O concentrations, and increasing atmospheric N deposition; (4) GE to test the sensitivity of N_2O sea-air fluxes to constant preindustrial atmospheric N_2O under increasing atmospheric CO_2 forcing and constant preindustrial atmospheric N deposition. All four model experiments were spun-up for 6000 years with preindustrial boundary conditions (solar and volcanic and aerosol forcing, fixed atmospheric CO_2 of 280 ppm and N_2O of 276 ppb, and preindustrial atmospheric N deposition), WARM and FULL simulations were forced with historical fossil fuel CO_2 emissions and atmospheric N_2O concentrations until 2005, simulations were extended until 2100 using the RCP8.5 scenario forced by anthropogenic CO_2 emissions and N_2O concentrations [*Meinshausen et al.*, 2011]. NDEP and FULL simulations account for the transient atmospheric N deposition forcing over the period 1850 until 2100 following RCP8.5, reconstructed using the multimodel mean of the Atmospheric Chemistry and Climate Model Intercomparison Project [*Lamarque et al.*, 2013]. GE was forced with the RCP8.5 anthropogenic CO_2 emissions but with constant preindustrial prescribed (276 ppbv) N_2O concentrations throughout the simulation.

3. Results

3.1. Warming: Changes in WARM

In the WARM simulation, CO_2-driven ocean surface warming (Figure 1a) reduces mixed layer depth globally by 22% in year 2100 relative to 1850 (Figure 1c). Warming-enhanced stratification (Figure 1a) reduces the supply of nutrients to the euphotic layer exacerbating phytoplankton NO_3 and PO_4 limitation (+18% and +20%, respectively) in low-latitude regions (here defined as 40°N:40°S) (Figure 1e, where nutrient limitation is calculated as $\mathrm{lim} = 1 - \frac{[\mathrm{nutrient}]}{[\mathrm{nutrient}]+K_{\mathrm{nut}}}$).

Our model projects a modest increase in global net primary production (NPP) of 1.2 Pg C y^{-1} (+2%) (Figure 1b), and a steady decline in export production (EP) ($\sim -7\%$) to 5.5 Pg C y^{-1} (Figure 1b) by the end of the century. NPP is projected to decrease particularly over the North Atlantic (13%) and to a less extent in the tropical Northwest Pacific, tropical Western Indian Ocean, and largely increase in the Southern Ocean (40%) and Arctic Ocean (Figure 2b). EP is projected to increase (7%) in high-latitude regions (Figure 2c), particularly over the Southern Ocean (+31%), and to decline in the North Atlantic and low-latitude regions (14%), except over the Eastern Equatorial Pacific. Increasing N limitation and higher temperatures promote up to +5% higher global N inputs by N_2 fixation (Figure 1d) until 2050. However thereafter, increasing P-limiting conditions lead to a N_2 fixation decline such that by 2100 fixed N_2 inputs are 126 Tg N y^{-1}, with little change relative to preindustrial times (Table 2). The N_2 fixation decline occurs in the oligotrophic Atlantic and subtropical western Pacific Ocean (Figure 2d).

By the end of the 21st century the global average ocean O_2 concentration (177 mmol m^{-3}) declines by 4.6% (Figure 1g), and oxygen minimum zones (OMZ, $O_2 < 5$ mmol m^{-3}) thicken and increase their volume by +21% (Figure 1h). The largest OMZ expansion occurs in the Northwestern Pacific ($+1 \cdot 10^6$ km^3) and is associated with OMZ thickening (Figure 2j). Minor increases occur in the Indian Ocean, and little net change occurs in the Eastern Tropical Pacific (ETP) (Figure 2j).

Water column denitrification (WCD) increases by 6% to the global integrated value of 75 Tg N y^{-1} (Figure 1f). The largest increase occurs in the Northwestern Pacific (Figure 2g). Conversely, benthic denitrification (BD)

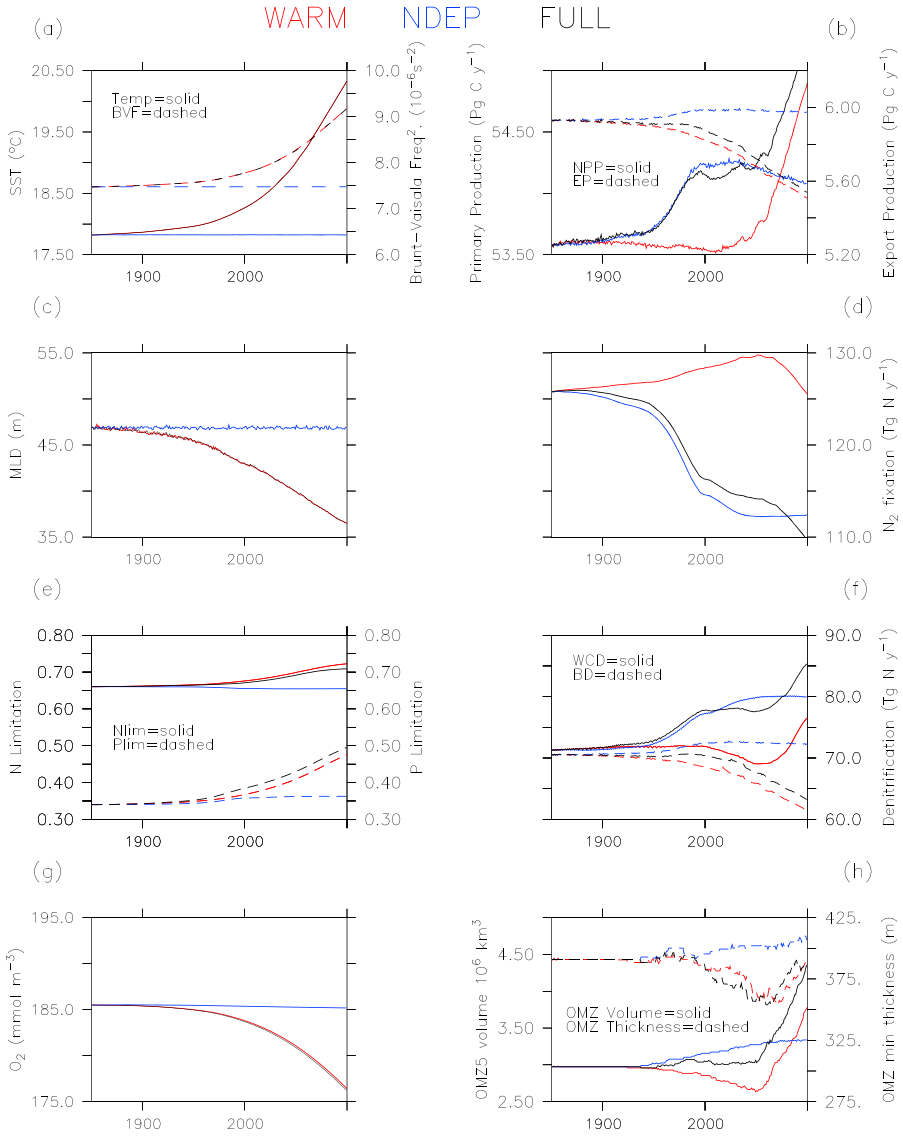

Figure 1. Projected changes in the model simulations WARM, NDEP, and FULL of (a) global average surface temperature (°C) (solid) and squared Brunt-Vaisala Frequency (10^{-6} s^{-1}) (dashed) as stratification index; (b) global integrated net primary (solid) and export (dashed) production at 100 m (Pg C y^{-1}); (c) global and annually averaged mixed layer depth, MLD (m) calculated using the 0.125 density criterion; (d) global integrated N_2 fixation (Tg N y^{-1}); (e) low-latitude (40°S:40°N) arithmetic average of NO_3 (solid) and PO_4 (dashed) limitation; (f) global integrated WCD (solid) and BD (dashed) (Tg N y^{-1}); (g) global mean O_2 (mmol O_2 m^{-3}); (h) OMZ (O_2 < 5 mmol m^{-3}) volume (10^6 km^3) (solid) and OMZ thickness (m) (dashed). Please note that in Figures 1a, 1c, and 1g results from FULL (black lines) are almost identical to results from WARM (red lines), and hence, black lines overprint red lines. Nonfixing phytoplankton and diazotrophs have the same half-saturation constants for PO_4 (Table 1), implying same P limitation.

is reduced everywhere (Figure 2h) to 8.6 Tg N y^{-1} (−12%) in 2100 (Figure 1f), with the exception of high-latitude regions.

Our WARM model experiment projects a (5%) decline in total subsurface N_2O production (0.84 Tg N y^{-1}, Figure 3b) and a 24% global decline in the oceanic N_2O emissions to 2.7 Tg N y^{-1} (Figure 3a) by the end of the century. The largest decline occurs in the Northwestern Atlantic and Pacific Oceans and in the 40°S–60°S latitudinal band (Figure 2l).

3.2. Increasing Atmospheric N Deposition: Changes in NDEP

Atmospheric N deposition is largest over the Northern Hemisphere (19 Tg N y^{-1}) (Figure 4a), reflecting intensified anthropogenic activities. The increase of atmospheric N deposition to the ocean of 27 Tg N y^{-1} (+165%) in year 2100 has little effect on relieving N limitation relative to preindustrial conditions (Figures 1c and 4e).

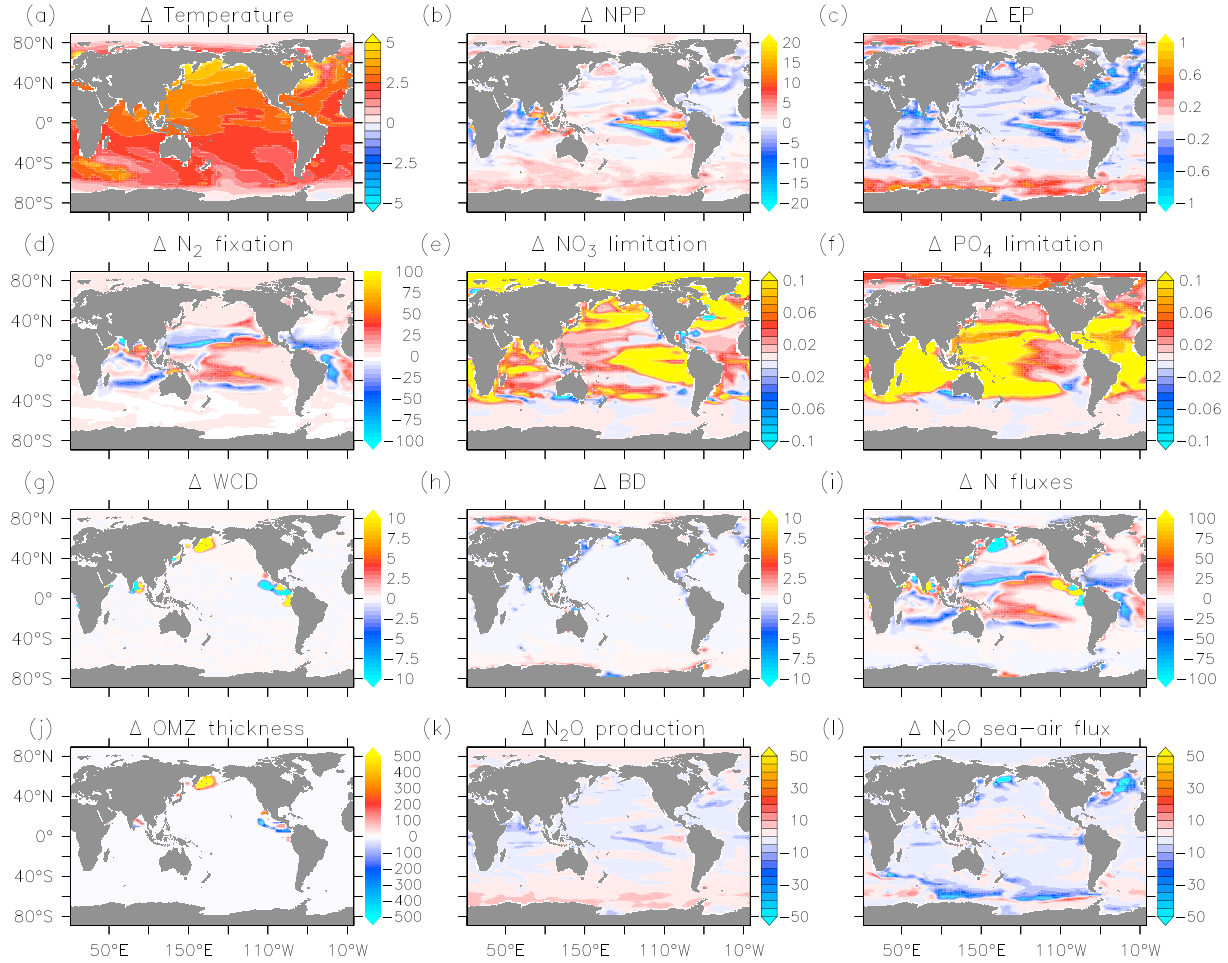

Figure 2. Change between the averaged 2090–2100 and 1850–1860 time periods in WARM of (a) sea surface temperature (°C); (b) NPP (mol C $m^{-2}y^{-1}$); (c) EP (mol C $m^{-2}y^{-1}$); (d) N_2 fixation (mmol N m^{-2} y^{-1}); (e) NO_3 limitation; (f) PO_4 limitation; (g) WCD (mmol N m^{-2} y^{-1}); (h) BD (mmol N m^{-2} y^{-1}); (i) N Flux (Ndep + N2 fix − WCD − BD) (mmol N m^{-2} y^{-1}); (j) OMZ thickness (m); (k) N_2O production (mmol N_2O m^{-2} y^{-1}); (l) oceanic N_2O emissions (positive upward)(mmol N_2O m^{-2} y^{-1}). Total N_2O production = low-O_2 pathway + high-O_2 pathway. Nonfixing phytoplankton and diazotrophs have the same half-saturation constants for PO_4 (Table 1), implying same P limitation.

Table 2. End of the 21st Century Average (2090–2100 Average Period) and Percent Change (in Parenthesis, %) Relative to Preindustrial Conditions (1850–1860 Time Average) of Model Experiments WARM, NDEP, and FULL Processes

Processes	Unit	WARM	NDEP	FULL
NPP	Pg C y^{-1}	54.8 (+2.2)	54.1 (+1)	55.1 (+3)
EP	Pg C y^{-1}	5.5 (−7)	5.9 (+1)	5.6 (−6.3)
N_2 fixation	Tg N y^{-1}	126 (+0.3)	112 (−10)	110 (−12.5)
WCDen	Tg N y^{-1}	75 (+6)	80 (+12)	84 (+18)
BDen	Tg N y^{-1}	62 (−12)	72 (+2.5)	64 (−10)
N deposition	Tg N y^{-1}	16 (0)	43 (+165)	43 (+165)
N cycle imbalance	Tg N y^{-1}	+5.1	+2.9	+5.3
ΔN inventory	%	+0.16	+0.11	+0.24
OMZ volume (O_2 < 5 mmol m^{-3})	10^6 km^3	3.6 (+25)	3.3 (+10)	4.2 (+45)
ΔN_2O inventory	%	+4.5	−0.1	+4.2
N_2O oceanic emissions	Tg N y^{-1}	2.68 (−24)	3.51 (+0.8)	2.65 (−24.5)

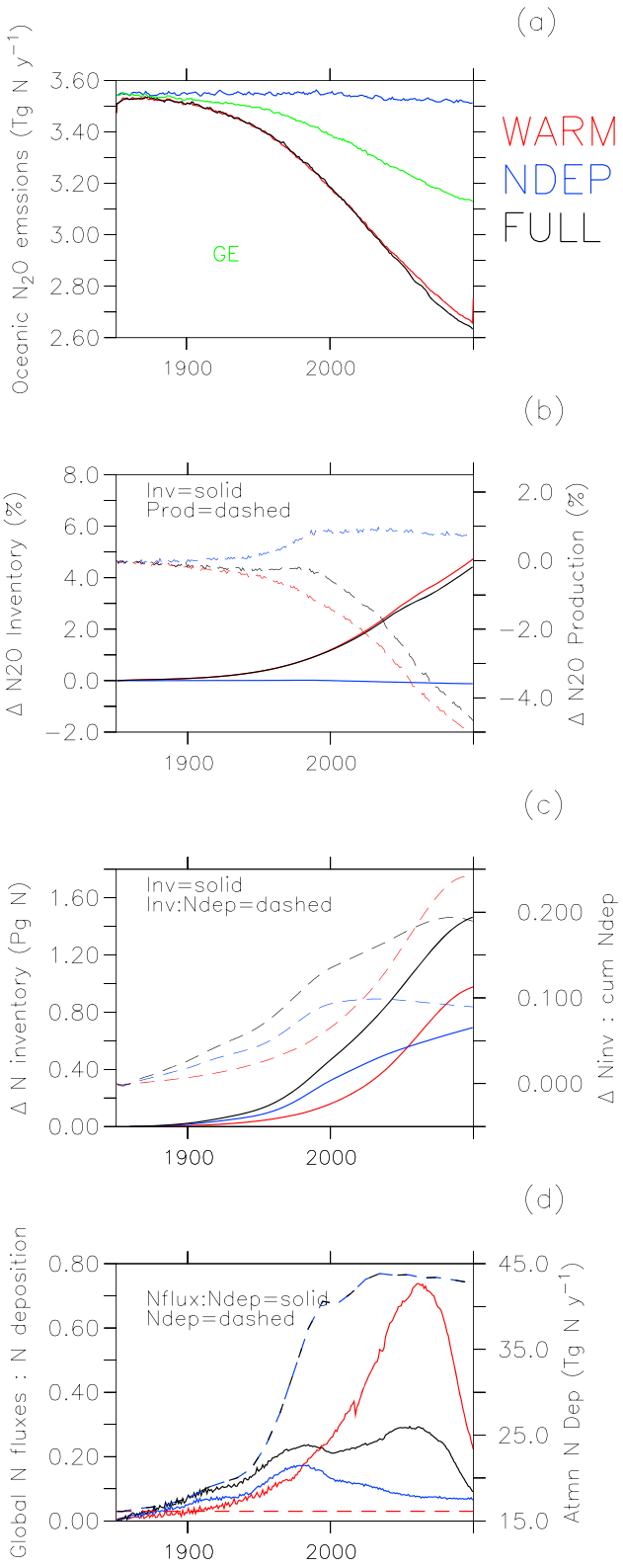

Figure 3. Projected changes in model simulations WARM, NDEP, and FULL of (a) global integrated oceanic N_2O emissions (Tg N y^{-1}) (positive upward), green solid line is from sensitivity experiment GE; (b) percent change in N_2O inventory (solid), and N_2O production change (%) (dashed); (c) N inventory change (Pg N) (solid), N inventory change relative to cumulative N deposition (dashed); (d) fraction of global N fluxes (N inputs − N outputs) relative to atmospheric N deposition (solid) and integrated atmospheric N deposition (Tg N y^{-1}) (dashed).

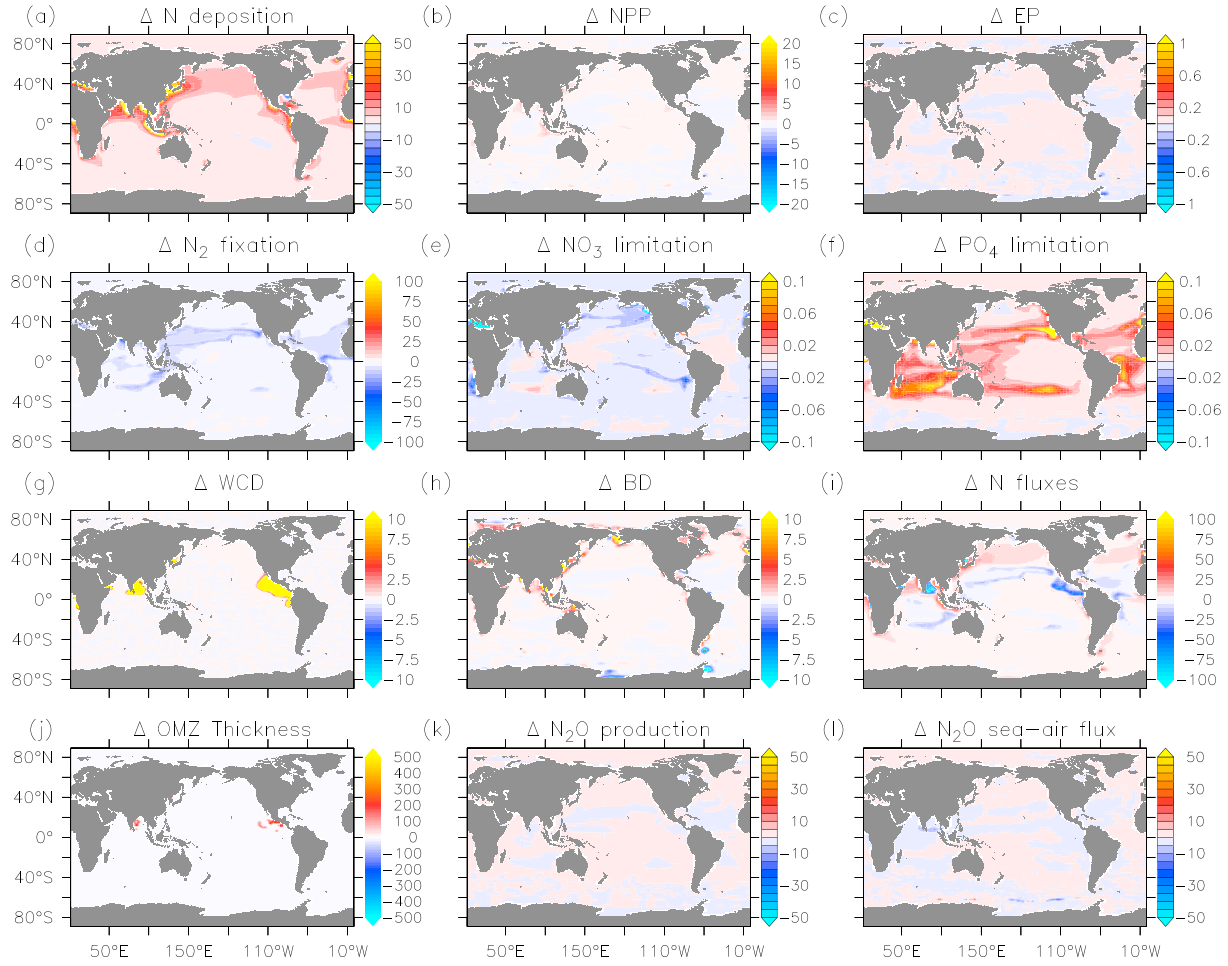

Figure 4. Change between the averaged 2090–2100 and 1850–1860 time periods in NDEP of (a) atmospheric N deposition (mmol N m^{-2} y^{-1}); (b) NPP (mol C m^{-2} y^{-1}); (c) EP (mol C m^{-2} y^{-1}); (d) N_2 fixation (mmol N m^{-2} y^{-1}); (e) NO_3 limitation; (f) PO_4 limitation; (g) WCD (mmol N m^{-2} y^{-1}); (h) BD (mmol N m^{-2} y^{-1}); (i) N Flux (Ndep + N_2 fix − WCD − BD) (mmol N m^{-2} y^{-1}); (j) OMZ thickness (m); (k) N_2O production (mmol N_2O m^{-2} y^{-1}); (l) oceanic N_2O emissions (positive upward)(mmol N_2O m^{-2} y^{-1}). Total N_2O production = low-O_2 pathway + high-O_2 pathway. Nonfixing phytoplankton and diazotrophs have the same half-saturation constants for PO_4 (Table 1), implying same P limitation.

NPP increase is modest (+0.51 Pg C y^{-1}) (~1% relative to preindustrial times 55 Pg C y^{-1}) and results in an equivalent small increase in global EP and remineralization (Figures 1b and 6a). NPP and EP both decline in the subtropical North Atlantic and subtropical Northwestern Pacific Oceans, in response to higher N limitation relative to preindustrial conditions (Figures 4b and 4c). N inputs by marine N_2 fixation are reduced throughout the ocean (Figure 4d), leading to the global decline of 13 Tg N y^{-1}, −11% relative to preindustrial conditions. In the oligotrophic western Atlantic and North Pacific Oceans, combined regional N inputs from N_2 fixation and atmospheric N deposition decline relative to preindustrial conditions (Figure 4i).

The local increase of organic matter export above OMZs (8%) promotes additional O_2 consumption leading to a 12% expansion of OMZs occurring in the ETP (+0.3 · 10^6 km^3) and the Bay of Bengal (+0.1 · 10^6 km^3), triggering N loss by water column (8 Tg N y^{-1}, +12%) and benthic (2 Tg N y^{-1}, +3%) denitrification in these regions (Figures 4g and 4h).

Atmospheric N deposition does not significantly affect oceanic N_2O emissions (3.5 Tg N y^{-1}) in 2100 relative to preindustrial conditions (Figure 3a), and the N_2O inventory remains virtually unchanged (−0.1%)(Figure 3b and Table 2).

3.3. Combined Warming and Increasing Atmospheric N Deposition: Changes in FULL

In the FULL simulation, the deposition of N to the surface ocean counteracts to some extent enhanced NO_3 limitation from intensified stratification in a warming ocean. Thus, N limitation is less (−2%) stringent

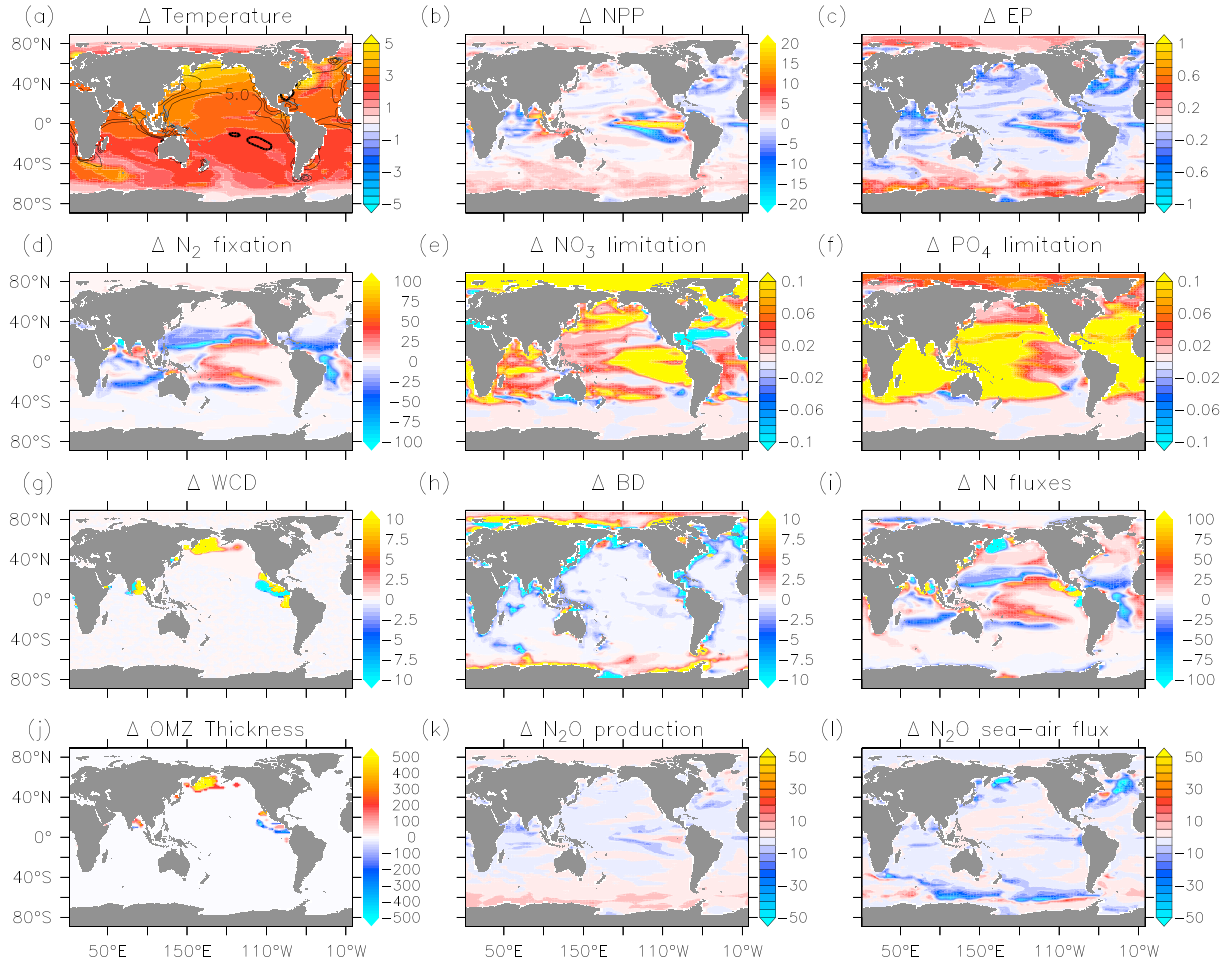

Figure 5. Change between the averaged 2090–2100 and 1850–1860 time periods in FULL of (a) sea surface temperature (°C) and contours of atmospheric N deposition (m^{-2} y^{-1}) (b) NPP (mol C m^{-2} y^{-1}); (c) EP (mol C m^{-2} y^{-1}); (d) N_2 fixation (mmol N m^{-2} y^{-1}); (e) NO_3 limitation; (f) PO_4 limitation; (g) WCD (mmol N m^{-2} y^{-1}); (h) BD (mmol N m^{-2} y^{-1}); (i) N Flux (Ndep + N_2 fix − WCD − BD) (mmol N m^{-2} y^{-1}); (j) OMZ thickness (m); (k) N_2O production (mmol N_2O m^{-2} y^{-1}); (l) oceanic N_2O emissions (positive upward)(mmol N_2O m^{-2} y^{-1}). Total N_2O production = low-O_2 pathway + high-O_2 pathway. Nonfixing phytoplankton and diazotrophs have the same half-saturation constants for PO_4 (Table 1), implying same P limitation.

in the FULL experiment relative to the WARM experiment, whereas P limitation is further intensified (+2%) (Figure 1e).

Ocean warming and increased atmospheric N deposition both support additional NPP, particularly in the high-latitude regions and in the ETP (Figure 5b), but the global increase to 55 Pg C y^{-1} by the end of the 21st century is modest (2.9%) (Figure 1b). In FULL, the high-latitude increase in EP is overcompensated by the decline in most low-latitude regions (Figure 5c), thereby leading to a 6% decline in global EP over the 21st century. Atmospheric N inputs further augment the warming-induced increase in P limitation (Figure 5f). This reduces the niche of marine N_2 fixers (Figure 5d) in the tropical and subtropical North Pacific and North Atlantic Oceans, decreasing N_2 fixation by ~12% by 2100 in the FULL simulation (Figure 7 and Table 2).

In FULL, a large (+45%) expansion of the OMZ volume is projected by the end of the 21st century, which is larger than the linear combination of the OMZ expansion in WARM and NDEP (Figure 1h). The largest expansion occurs in the western North Pacific (Figure 5j). Water column denitrification is intensified by +18% relative to preindustrial conditions, particularly in the North Pacific Ocean (Figure 5g). The increase of benthic denitrification in the high latitudes is counteracted by a decline in the rest of the ocean (Figure 5h), leading to a 10% contraction of global BD by 2100 (7 Tg N y^{-1}, Figure 1f). By the end of the century, total N_2O production is projected to decline by 5% and N_2O emissions are reduced by 24% (Figures 3a and 3b).

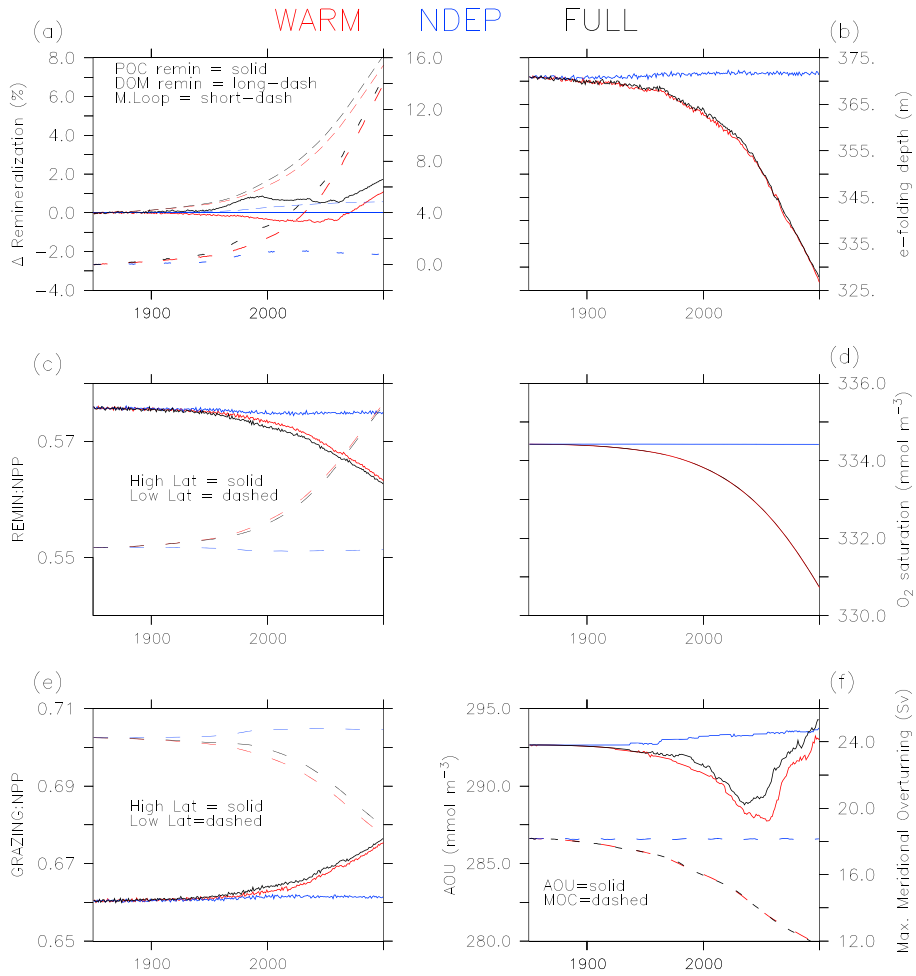

Figure 6. Projected changes in model simulations WARM, NDEP, and FULL of (a) percent change of POC remineralization (solid), DOC remineralization (long dash) (left *y* axis) and microbial loop (short dashed, right *y* axis); (b) remineralization *e*-folding depth (m); (c) fraction of remineralization relative to NPP in high-latitude (solid) and low-latitude regions (dashed); (d) O_2 (mmol O_2 m^{-3}) saturation; (e) fraction of grazing relative to NPP in high-latitude (solid) and low-latitude regions (dashed); (g) AOU (mmol O_2 m^{-3}) in OMZ (solid) and maximum meridional overturning circulation (MOC) (Sv) (dashed);

4. Discussion

4.1. Warming Effects on Ocean Biogeochemistry

The slight NPP increase in our model simulation WARM is in contrast with the projected decline simulated in most of the CMIP5 models, although these models have a large spread 2%–13% [*Bopp et al.*, 2013], which was attributed to the reduction of surface nutrients resupply resulting from enhanced stratification [*Steinacher et al.*, 2010; *Bopp et al.*, 2013] and stronger top-down control [*Laufkötter et al.*, 2015]. Our result is consistent with other studies that find an increase in NPP (~5%), when direct effects of warming on metabolic processes such as growth and remineralization are accounted for [*Schmittner et al.*, 2008; *Taucher and Oschlies*, 2011]. In our simulation, warming promotes increased particulate (1%) and dissolved (8%) organic matter remineralization and microbial loop recycling (~15%)(Figure 6a) that can support phytoplankton recycled production, as found in previous modeling studies [*Taucher and Oschlies*, 2011]. In some CMIP5 models, however, temperature-enhanced growth rates of phytoplankton are offset by temperature-enhanced losses of phytoplankton via grazing, leading to a decrease in NPP and suggesting elevated sensitivity of NPP to temperature dependencies in model parameterizations [*Laufkötter et al.*, 2015].

Generally, the regional patterns of projected NPP changes are consistent with the regional sign of change in all CMIP5 models except for the eastern Equatorial Pacific region consistent with only few CMIP5 models (GFDL-ESMs and CESM1-BGC) [*Bopp et al.*, 2013]. To identify the reasons of NPP spatial variability, in our model,

Table 3. Area Extension (%) of the Factors Most Limiting Growth of Phytoplankton and Diazotrophs, in Years 1850 and 2100 for Model Experiments WARM and NDEP

WARM	Most Limiting Factor	1850	2100	Sign of Change
Phytoplankton				
	N	53	58	+
	P	0.04	2.4	+
	Fe	40	34	–
	Temp	1.6	1	–
	Light	2.4	1.6	–
Diazotrophs				
	P	23	38	+
	Fe	59	49	–
	Temp	14	10	–
	Light	0.3	<0.3	–
NDEP				
Phytoplankton				
	N	52.8	52.6	–
	P	0.04	0.4	+
	Fe	40	40.6	+
	Temp	1.6	<1	–
	Light	2.4	3	+
Diazotrophs				
	P	23	26	+
	Fe	59	69	+
	Temp	14	2.4	–
	Light	0.3	0.17	–

we investigate the factors that control the growth rates of phytoplankton (temperature, light, and nutrient limitation, i.e., bottom-up control) and loss terms driven by grazing (top-down control).

Phytoplankton growth depends on a temperature-dependent factor that is projected to increase everywhere (global average +2%, Figure S1d) following a north-south gradient, caused by the stronger surface warming of the Northern Hemisphere (Figure 2a). Light limitation (Figure S1e) is projected to decline in high latitudes due to shallower MLDs (Figure S1b), particularly in the Southern Ocean and further by the reduction in the sea ice fraction (Figure S1a). Both factors contribute to increased phytoplankton growth rates in the high latitudes in our model (Figure S1f). While increased vertical stratification and shoaling of the MLD exacerbate nitrate and phosphate limitation in surface layers, the warming-driven increase in the upper ocean remineralization, which is most intense in low-latitude regions that experience higher temperatures (Figure 6c), somehow counteracts the surface nutrient decline, leading to complex regional patterns (Figures 2e and 2f). N-limited areas expand from 53% to 58%, while Fe-limited areas contract. Also P limitation increases in the Western North Atlantic (Table 3, Figures S2a and S2b), consistent with the earlier study by *J. K. Moore et al.* [2013]. The resulting pattern of phytoplankton growth rate is complex in low-latitude regions, with reduced phytoplankton growth rates in the tropical and subtropical Atlantic Ocean and South Pacific subtropical gyre and large variability elsewhere (Figure S1f).

The temperature-dependent zooplankton growth rates (Figure S1g) increase everywhere due to surface warming. However, as zooplankton grazing rates are capped for temperatures above 20°C in our model configuration, the highest increase in zooplankton growth rates occurs in subpolar regions, particularly in the Northern Hemisphere, while their increase in the low-latitudinal band is limited (Figure 6e). This pattern affects zooplankton grazing (Figure S1h), contributing to generate further complexity in the regional patterns in our modeled NPP, in support of a top-down control of NPP variability [*Laufkötter et al.*, 2015], with stronger top-down control in the high latitudes relative to the low latitudes in our model (Figure 6e).

Diazotroph's maximum growth rate increases with higher temperatures, particularly over the Northern Hemisphere (Figure S1j). Although temperature and Fe-limited regions shrink (Table 3, Figures S3a and S3d), diazotroph's growth becomes more limited by PO_4 availability in the tropical and subtropical Atlantic, Western Pacific, and Indian Oceans (Figure S1k). Thus, in our model with prescribed iron limitation, temperature-enhanced growth rates are offset by stratification-induced increased PO_4 limitation, limiting N_2 fixation increase only to waters receiving sufficient P.

In our model, the warming-driven changes in remineralization lead to the shoaling of the depth of particle remineralization globally by 40 m (−11%) (also known as the remineralization *e*-folding depth) (Figure 6b). In previous idealized model studies, which did not account for the warming-driven circulation changes, the temperature-driven shoaling of remineralization (and decrease in *e*-folding depths) lead to the increase in surface nutrient availability [*Matsumoto*, 2007; *Segschneider and Bendtsen*, 2013]. In our simulation, however, this effect is offset by reduced surface nutrient resupply due to enhanced stratification, leading to a monotonic increase of surface nutrients limitation (Figures 1e, 2e, and 2f). The resulting overall effect of warming in our simulation is a 7% decline in EP by 2100, well within the range of current climate model (CMIP5) estimates of projected 21st century EP decline (1 to 18%) [*Bopp et al.*, 2013; *Laufkötter et al.*, 2016]. We did not consider, however, the warming-driven changes in viscosity, which may lead to faster sinking particles in a warmer ocean, increasing the remineralization depth on centennial to millennial time scales [*Taucher et al.*, 2014]. Similarly, phytoplankton community restructuring toward the fast-sinking calcifiers may remove nutrients more efficiently from the surface ocean to depth [*Kvale et al.*, 2015]. On the other hand, calcium carbonate production may be attenuated due to ongoing acidification [*de Jesus Mendes and Thomsen*, 2012]. The combined net effects of these processes on the partitioning of nutrients between the surface and deep ocean requires further study.

The global decline in oceanic O_2 content in WARM is in line with CMIP5 Earth system climate models projections (1.5%–4%). This decline is related to warming-driven reduction in O_2 solubility and ventilation, and associated with the projected slow down of the meridional overturning circulation (Figures 6d and 6f). While the simulated global decline of O_2 is consistent with observations [*Stramma et al.*, 2008, 2012; *Schmidtko et al.*, 2017], significant model data regional discrepancies occur, possibly related to the natural forcing variability that is currently not represented within most models [*Schmidtko et al.*, 2017]. The temporal variability of OMZ volumes projected by our study may be explained by the combination of reduced O_2 biological consumption, the warming-driven decline in O_2 solubility, ventilation, and circulation slowdown (Figures 6d and 6f). This is suggested by the changes in apparent oxygen utilization (AOU) within the OMZ, which respond to the biological O_2 consumption and ventilation rate and circulation change. As organic matter export is reduced throughout the tropics and subtropics, AOU declines. This trend is compensated for by circulation slowdown and associated reduced ventilation that increases AOU by 2100. These processes, together with poor representation of OMZs in global coarse climate-biogeochemical models, have been suggested to explain the small net change of OMZ volumes in many CMIP5 models [*Bopp et al.*, 2013; *Cocco et al.*, 2013; *Cabre et al.*, 2015]. Although the inclusion of an equatorial isopycnal mixing scheme, mimicking the transport of oxygen and nutrients by zonal jets [*Getzlaff and Dietze*, 2013], has allowed our model to simulate contemporary suboxic volumes ($2.75 \cdot 10^6$ km^3) within observational uncertainties ($2.45–4.13 \cdot 10^6$ km^3) [*Bianchi et al.*, 2012], the locations of OMZs are still too close to the equator and do not capture the complexity of the Arabian Sea and Bay of Bengal, thus, our model projections should be interpreted with caution.

4.1.1. Warming Triggers N Cycle Feedbacks

In WARM, warmer and more N-limited surface waters are insufficient to favor diazotroph's growth, as hypothesized by previous studies [*Dutkiewicz et al.*, 2014], because of increasing P-limited areas (26%, Figures S3a and S3d). We acknowledge that our prescribed Fe concentrations could lead to a different sensitivity of the diazotrophs.

Water column denitrification increases due to the expansion of OMZs. In contrast, previous studies have projected small net changes or even a contraction of OMZ's [*Bopp et al.*, 2013; *Cabre et al.*, 2015], suggesting a possible decrease in WCD under ocean warming [*Oschlies et al.*, 2008]. Unique to this study is the projected global decline in BD, which results from the warming-driven reduction in EP. Though some CMIP5-models include benthic denitrification parameterizations, the lack of dedicated N cycle studies does not allow our BD projection to be compared with earlier results. Overall, our model predicts a small N_2 fixation change and the compensation of the increased N loss by water column denitrification with declining N loss by benthic denitrification (Figure 8). This results in a small positive N flux imbalance (Figure 7), and a fairly small N inventory

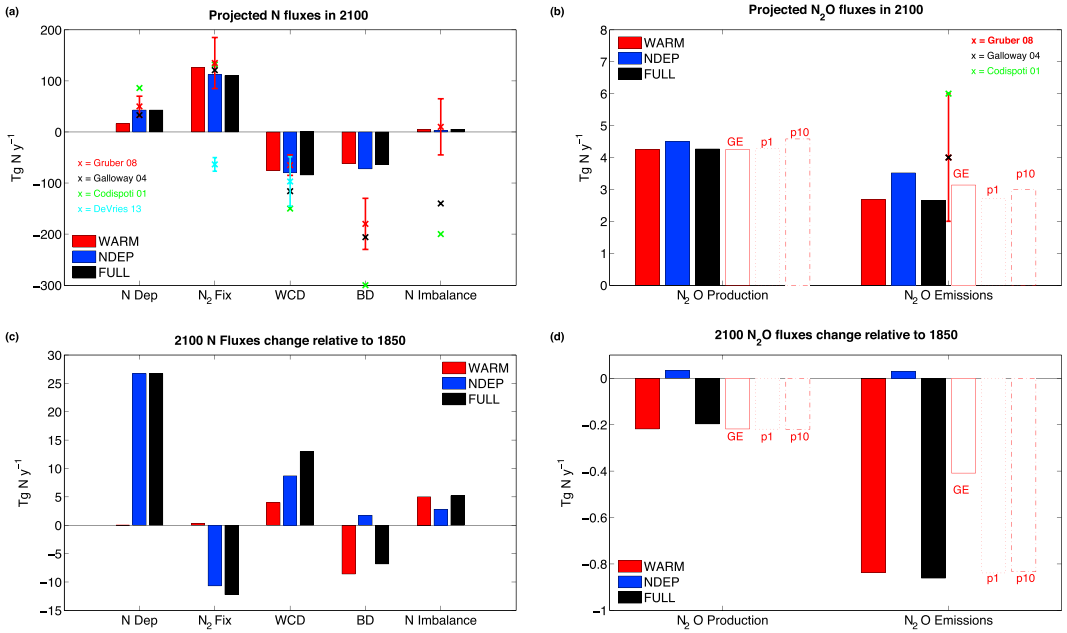

Figure 7. Projected 2100 global average (2090–2100 averaged period) of (a) N fluxes from N deposition (N dep), N_2 fixation (N_2 fix), water column denitrification (WCD), benthic denitrification (BD) and N flux imbalance (Tg N y^{-1}); (b) N_2O production and oceanic emissions (Tg N y^{-1}). Changes relative to preindustrial (2090–2100 and 1850–1860 average time periods) of (c) N fluxes (Tg N y^{-1}) and (d) N_2O Flux (Tg N y^{-1}) in WARM, NDEP, and FULL simulations. N_2O sensitivity experiments: GE, N2Op1, and N2Op10 are reported for comparison. Current estimates and associated error of N fluxes and N_2O emissions from *Codispoti et al.* [2001], *Galloway et al.* [2004], *Gruber* [2008], and *DeVries et al.* [2013] are reported for comparison.

change by 2100 (Figure 3c and Table 2), suggesting that marine N cycle feedbacks can help stabilize the N inventory under global warming.

4.1.2. Warming Effects on the N_2O Cycle

The sign of change, in response to global warming, of our projected N_2O emission is consistent with the global modeling work of *Martinez-Rey et al.* [2015]. The decline in oceanic N_2O emissions of about 24% observed in our study is larger than the 4 to 12% decline predicted by that earlier study [*Martinez-Rey et al.*, 2015]. This discrepancy is due to the increasing atmospheric N_2O concentrations in our model simulation that affect the air-sea N_2O gradient contributing to a further ~10% reduction in oceanic emissions. This is assessed by comparing WARM with the sensitivity experiment GE (atmospheric N_2O concentrations constant at preindustrial level) (Figure 3a, compare green and red solid lines). The latter shows a much smaller decline in oceanic N_2O emissions, similarly to what is found by *Martinez-Rey et al.* [2015]. The warming-driven decrease in N_2O solubility is counteracted by enhanced N_2O equilibrium surface concentration as atmospheric N_2O concentrations increase. Warming-induced enhancement of marine stratification and a slowdown of circulation, as inferred from the decline in the maximum overturning circulation (Figure 6f) also reduces N_2O emissions. These processes explain the increase in N_2O inventory (+4.5%, Figures 3a and 3b) despite that subsurface N_2O production is projected to decline. While our diagnosed N_2O production via the low-O_2 pathway is projected to increase in response to ocean deoxygenation, the decline in N_2O production via the high-O_2 pathway, due to the reduction in export production, is larger and drives the total N_2O production decrease in our model (Figure 8). The larger contribution of high-O_2 production pathway is associated with aerobic subsurface remineralization of organic matter occurring in the majority of the ocean's volume. As configured in our model, surface N_2O production is inhibited. As a consequence, regional changes in N_2O production (Figure 2k) are closely associated with changes in regional export production (Figure 2c) [see also *Martinez-Rey et al.*, 2015]. Any changes in surface N_2O production, associated with remineralization occurring in the surface layer, might effect future emissions and will be discussed in section 5.2.

4.2. Effects of Increasing Atmospheric N Deposition

In our simulation, increasing atmospheric N deposition has a modest effect on global oceanic NPP and EP. The small (~1%) N fertilization effect on global EP, inferred in this study, is lower than that suggested by a

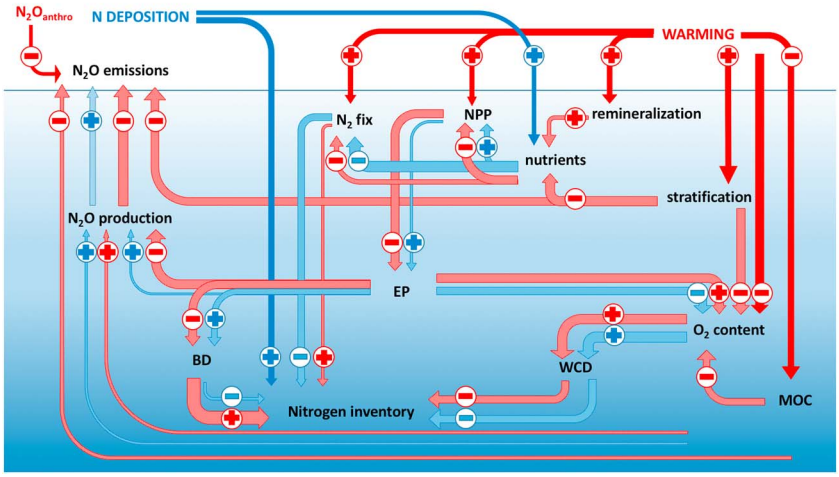

Figure 8. Schematic of the biogeochemical feedbacks and their sign of change associated with warming and increased N deposition. Solid lines represent direct effects, light-colored lines represent indirect effects. Thickness of the lines represent, in a semiquantitative way, the intensity of the perturbation. Warming directly enhances metabolic rates (net primary production (NPP), N_2 fixation (N_2 fix), and remineralization) and stratification and reduces O_2 solubility and meridional overturning circulation (MOC). Intensified stratification reduces ocean ventilation driving additional O_2 decline and limits the supply of new nutrients in the euphotic zone. This contrasts the enhanced surface nutrient availability due to faster remineralization and the higher growth rates, resulting in little net change of NPP and N_2 fix. Reduced new nutrient inputs lead to a decline in export production (EP), which in turn reduce benthic denitrification (BD) and O_2 consumption at depth. However, the combination of the warming-driven processes results in a net O_2 reduction, which intensifies water column denitrification (WCD). More N loss via WCD compensated by less N loss via BD and small changes in N_2 fix result in little net N inventory change. N_2O production decline due to reduced EP is larger than the N_2O production increase in low-O_2 waters. This, together with stratification-reduced N_2O outgassing, circulation slowdown, and human-driven atmospheric N_2O increase (N_2O_{anthro}) contribute to reduce oceanic N_2O emissions (N_2O emissions). Nitrogen deposition stimulates NPP but reduces the niche of N_2 fixers with a small EP increase. This, in turn, stimulates BD and O_2 demand at depth that result in larger WCD. Overall, the atmospheric N inputs are compensated by more N loss via denitrification and reduced N_2 fix, with little net effect on N_2O production and oceanic emissions. For the combined perturbations, the net sign of change of each process is given by the sum of the signs scaled by the line thickness.

previous modeling study that did not include N_2 fixation feedbacks [*Suntharalingam et al.*, 2012], but it is consistent with more comprehensive earlier studies [*Krishnamurthy et al.*, 2007, 2009; *Somes et al.*, 2016; *Yang and Gruber*, 2016] (Table 1). The limited impact of atmospheric deposition on ocean productivity is due to the presence of strong N cycle feedbacks, accounted for in our model. N additions reduce the ability of N_2 fixers to compete with nonfixing phytoplankton for P and Fe [*Landolfi et al.*, 2015] by expanding the regions of P and Fe limitation by 13% and 17%, respectively (Table 3), which result in reduced N inputs by diazotrophs (Figure 4d). In some regions, the decline in N_2 fixation is larger than the increase in N deposition, leading to a negative N flux balance (Figure 4i). Idealized model experiments of local N additions in light or iron-limited high-latitude regions by *Somes et al.* [2016] showed that these waters eventually recirculated into the subtropics driving additional P and Fe limitation there, resulting in a reduction of N_2 fixation on decadal to centennial time scales. This suggests that local nutrient limitation patterns are affected by large-scale circulation. In our study, this results in the counterintuitive increase of N limitation in response to N deposition that leads to the decline in PP and EP in the subtropical North Atlantic and subtropical Northwestern Pacific Oceans.

Although atmospheric N additions have a very modest impact on a global scale, N additions in proximity of Fe-replete OMZs and poorly oxygenated continental shelves stimulate organic matter production, which, when exported to depth, is remineralized under low O_2 conditions via denitrification. The WCD (12%) and BD (3%) increase predicted under increasing atmospheric N deposition in this study is similar to the changes simulated previously [*Yang and Gruber*, 2016]. As denitrification consumes about 7 moles of NO_3 per mole of remineralized nitrogen, this regional process can lead to net local N loss [*Somes et al.*, 2016], and impact the global N inventory [*Landolfi et al.*, 2013]. In our model, this explains why the N flux balance (N deposition + N_2 fixation − WCD − BD) in NDEP has the smallest N surplus relative to WARM despite the much reduced N deposition in this latter simulation (Figure 3d), and the N inventory increase in NDEP is smaller relative to

the WARM and FULL simulations (Figure 3c). Globally, increased N inputs via atmospheric N deposition are compensated for by reduced N_2 fixation rates and enhanced N loss by denitrification (Figure 8), resulting in a small positive N flux imbalance of +2.8 Tg N y^{-1} (Table 2). This N increase is only ~7% of the deposited N, implying a negligible N inventory changes by the end of the century (Figure 7 and Table 2).

The very modest impact of N deposition on ocean productivity results also in little change of oceanic N_2O emissions (less than 1%), similar to estimates from *Zamora and Oschlies* [2014] but smaller than the 3–4% increase suggested by *Suntharalingam et al.* [2012]. Our predicted smaller impact is related to the smaller N deposition effect on both NPP and EP in this study (1%) relative to the earlier study (3–4%) [*Suntharalingam et al.*, 2012]. This difference in model predictions is due to accounting for N cycle feedbacks, which are neglected in *Suntharalingam et al.* [2012].

4.3. Combined Warming and Atmospheric N Deposition Effects

The biogeochemical changes triggered by ocean warming are larger than those stimulated by increasing atmospheric N deposition (Table 2 and Figure 8). The combined perturbations intensify the increase of NPP in the FULL model prediction relative to the individual perturbations. However, the predominant effect of warming on declining EP largely offsets the small increase lead by atmospheric N fertilization, resulting in a net, albeit smaller, decline EP in FULL relative to WARM perturbation alone. The magnitudes and sign of change of global NPP and EP in our simulation are consistent with the range of variability occurring among CMIP5 models [*Bopp et al.*, 2013], but agree less with the previous study of *J. K. Moore et al.* [2013], also accounting for the combined effects of RCP8.5 warming and N deposition, which found a more intense decline in both NPP and EP (5.7% and 13%, respectively). A possible factor contributing to this discrepancy is the warming-induced increase and shoaling of remineralization in our model configuration that (i) support NPP increase based on regenerated surface nutrients and (ii) displace remineralized nutrients closer to the surface layer, leading to the less intense decline in export production in our model simulation relative to the study by *J. K. Moore et al.* [2013]. Similar discrepancies among model simulations with and without temperature-dependent remineralization have been found in the model study of *Taucher and Oschlies* [2011]. However, other factors, such as differences in initial conditions or different model sensitivity to nutrient limitation, grazing pressure, and warming, may also cause the differences with the earlier study.

The combined perturbations expand diazotroph's P- and Fe-limited regions (Figure S3f and Table 3), reducing N_2 fixation activity by about 13%. While this reduction is smaller but in line (~20%) with the findings of *J. K. Moore et al.* [2013], the underlying mechanism is somehow different. In that earlier study, which includes an explicit dynamic iron cycling, iron-limited areas were found to shrink (26%), whereas P-limited regions doubled [*J. K. Moore et al.*, 2013].

The projected OMZ volume increase under combined RCP8.5 warming and N deposition is in line with the study of *J. K. Moore et al.* [2013]. However, our simulated OMZ volume change is much reduced relative to that earlier study. While our model estimates of contemporary suboxic volumes are within the range of observational estimates [*Bianchi et al.*, 2012], the correct model sensitivity to predict future OMZ variability is not guaranteed. There are several potential deficiencies of medium-complexity coarse-resolution model that need to be considered. For example, simulated oxygen trends appear very sensitive to the preconditioning and variability of wind-forcing [*Getzlaff et al.*, 2016]. Additionally, unaccounted perturbations (e.g., ocean acidification) and biogeochemical complexity (phytoplankton stoichiometric variability) not included here may further influence OMZ volume change.

While both ocean warming and atmospheric N deposition induce positive feedbacks on WCD via the expansion of OMZs, consistent with the findings from *J. K. Moore et al.* [2013], the warming-driven reduction in EP induces a negative feedback on BD in our model simulation. Although changes in export of organic matter are expected to impact on benthic denitrification rates [e.g., *Galbraith et al.*, 2013], earlier studies have not quantified BD 21st century projections hindering intermodel comparisons. In our simulations, the decline of N inputs via N_2 fixation, together with the compensation between increasing WCD and decreasing BD, results in a N flux imbalance of ~ +5 Tg N y^{-1} by the end of the 21st century under the combined perturbations. Over the centennial time scales considered in this study, this imbalance is far away from the hypothesized annual N deficit exceeding 100 Tg N y^{-1} [*Codispoti et al.*, 2001; *Codispoti*, 2007] and is virtually indistinguishable from present-day N flux estimate uncertainty [*Gruber*, 2004, 2008] (Figure 7). Our findings suggest that negative biogeochemical feedbacks limit the impact of anthropogenic perturbations on the N cycle and marine productivity.

For the RCP 8.5 scenario, oceanic production and emissions of N_2O are impacted more by warming than by atmospheric N deposition. While warming and atmospheric N deposition both expand OMZs and augment N_2O production under low-oxygen conditions, the warming-driven decline in export production yields a net reduction in total N_2O production, similar to an earlier warming-only study [*Martinez-Rey et al.*, 2015]. Enhanced stratification and reduced ocean ventilation both limit N_2O outgassing and explain the oceanic N_2O inventory increase (Table 2). With the increase of anthropogenic activities, atmospheric N_2O concentrations have been rising, leading to a greater N_2O surface equilibrium concentration in the ocean. Our results suggest that this process contributes to the N_2O emission reduction of about 10%. As human activities lead to increasing N_2O in the atmosphere, the ocean progressively dissolves more atmospheric N_2O.

5. Potential Caveats

5.1. Unaccounted Feedbacks on Ocean Biogeochemistry

There are several potential model caveats that need to be considered. Potential feedbacks on ocean biogeochemistry due to changes in iron availability, affected by atmospheric supply of iron and/or ocean circulation, have not been accounted for in this study, which lacks a fully prognostic iron model. While iron cycle parameterization in models have very large uncertainties [*Tagliabue et al.*, 2016], and the sign of future dust deposition is uncertain [*Mahowald and Luo*, 2003], a recent modeling study suggests that the anthropogenic enhancement of atmospheric iron deposition contributes to the tropical oxygen decline [*Ito et al.*, 2016], which could potentially exacerbate N loss and N_2O production via denitrification. Increased iron may favor the growth of marine N_2 fixers [*Dutkiewicz et al.*, 2014] in phosphorus-replete regions [*Landolfi et al.*, 2013], but with unknown effects on the N balance [*Landolfi et al.*, 2013] and ocean productivity. An earlier study, without accounting for warming, predicted that anthropogenic iron deposition stimulates more N_2 fixation than N deposition suppresses, but still with minor increases to marine production and export production [*Krishnamurthy et al.*, 2009]. The assessment of these feedbacks requires a further study with a fully prognostic iron model.

An additional caveat of our model, and most CMIP5 models, is that variations in the stoichiometry of phytoplankton [*Martiny et al.*, 2013] are neglected in current parameterizations. Phytoplankton stoichiometry exhibits large variability due to both environmental [*Klausmeier et al.*, 2004] and taxonomic factors [*Quigg et al.*, 2003]. High N:P requirements of oligotrophic phytoplankton has been found to exacerbate N limitation in the subtropical gyres favoring N_2 fixers [*Weber and Deutsch*, 2012]. In contrast, low N:P requirements of large rapidly growing phytoplankton may dampen N_2 fixers growth [*Mills and Arrigo*, 2010]. The variability of the elemental ratios of organic matter exported into the deep ocean may also lead to different sensitivities in projected carbon export and storage. The potential feedbacks and net effects of variable phytoplankton stoichiometry on ocean biogeochemistry remain unaccounted for in this study.

Lastly, in our model simulations we do not account for the potential effects of ocean acidification. This anthropogenically driven process is suggested to promote a restructuring of the phytoplankton community with possible advantages for marine N_2 fixers [*Hutchins et al.*, 2007; *Dutkiewicz et al.*, 2015]. On the other hand, ocean acidification may also lead to increased C:N phytoplankton uptake [*Riebesell et al.*, 2007] or to changes in organic matter ballast, that may augment the respiratory-O_2 demand at depth, promoting the expansion of OMZ [*Oschlies et al.*, 2008; *Hofmann and Schellnhuber*, 2009], affecting in turn water column denitrification and N_2O production-consumption balance.

5.2. Uncertainties in Modeling N_2O

There are large uncertainties in how best to parameterize marine N_2O models, and the choice of model parameterization might have large effects on N_2O projections. A previous analysis suggested that the largest uncertainty in N_2O emissions is the potential occurrence of surface N_2O production [*Zamora and Oschlies*, 2014]. Recent work provides some evidence that this process does occur [*Santoro et al.*, 2011; *Löscher et al.*, 2012; *Trimmer et al.*, 2016]. However, the in situ production pathways and environmental controls of surface N_2O production are still highly uncertain, and the rates of this process are unknown and difficult to constrain, in part, because any N_2O gas produced by biology in surface waters that is in excess of saturation values will be quickly emitted to the atmosphere, resulting in no visible surface water N_2O accumulation [*Zamora and Oschlies*, 2014]. In a highly idealized setting, we tested the effects of surface N_2O production on our N_2O projections performing two additional sensitivity experiments, N2Op1 and N2Op10, which, following *Zamora and Oschlies* [2014], allow 1% and 10% of surface N_2O production from nitrification, respectively.

While the decline in N_2O emissions is less pronounced with the occurrence of surface nitrification (20.5% to 22.5% decline compared to the 22.7% decline in WARM, Figure S4a), the projected sign of change is consistent among the different simulations (Figures 7b and 7d). In our highly idealized sensitivity experiments, projected N_2O emissions appear more sensitive to applying a constant atmospheric N_2O concentration than to including surface N_2O production (Figures 7b, 7d, and S4). The changes in total N_2O production and N_2O inventory also appear small (Figures S4b and S4c). This suggests that surface layer N_2O production has a modest impact relative to the production occurring in majority of the ocean's volume, giving us greater confidence in our N_2O projections. However, as a more quantitative understanding of this surface process becomes available, further scrutiny should follow.

Another uncertainty is the subsurface N_2O production parameterization, which locally may have very large impacts near OMZs [*Zamora and Oschlies*, 2014]. In this study, we use a linear N_2O production parameterization that increases linearly with decreasing O_2, which is based on in situ N_2O and AOU observations, intrinsically accounting for nitrification and denitrification N_2O production [*Zamora et al.*, 2012]. However, many earlier N_2O modeling studies [*Suntharalingam et al.*, 2000; *Nevison et al.*, 2003; *Jin and Gruber*, 2003; *Martinez-Rey et al.*, 2015] instead used a nonlinear parameterization originally or in part based on laboratory data from *Goreau et al.* [1980] in which N_2O production from nitrifying bacteria increases nonlinearly as O_2 declines. While a severely nonlinear parameterization based on *Goreau et al.* [1980] did not represent the observed N_2O concentrations in the ETP well [*Zamora et al.*, 2012], leading to high N_2O uncertainties within the UVIC2.9 model configuration [*Zamora and Oschlies*, 2014], the nonlinear parameterization of *Jin and Gruber* [2003], as modified by *Martinez-Rey et al.* [2015] is consistent with our modeled N_2O projections as discussed in section 4.1.2. The very high N_2O yield of nitrifying organisms under low-O_2 of *Goreau et al.* [1980] has been questioned by recent studies carried out under more realistic laboratory conditions [*Frame and Casciotti*, 2010; *Löscher et al.*, 2012] and in natural experimental settings [*Ji et al.*, 2015]. On the other hand, high-N_2O yield in low-O_2 waters from archaeal nitrification [*Trimmer et al.*, 2016] and denitrifying bacteria [*Arevalo-Martinez et al.*, 2015; *Babbin et al.*, 2015; *Kock et al.*, 2016] have been reported to cause very large N_2O surface accumulations associated with low-oxygen regions of the ETP. Future experimental work is required to assess the relative contribution of the different emerging microbial pathways and better constrain the environmental controls of N_2O production.

The next largest uncertainty in N_2O emissions is the O_2 concentration at which net N_2O is consumed during denitrification [*Zamora and Oschlies*, 2014]. This is due to the not well constrained O_2 sensitivity of N_2O reduction to N_2 during denitrification [*Zamora et al.*, 2012; *Babbin et al.*, 2015; *Ji et al.*, 2015]. Improving the mechanistic understanding of the sources and sinks of N_2O in the ocean is critical to develop explicit, process-based, model parameterization and improve the accuracy of N_2O projections.

6. Conclusions

We designed several model experiments to assess the individual and combined effects of rising temperatures and increasing anthropogenic N deposition on the marine N cycle over the 21st century. Our model projections suggest that biogeochemical processes respond more to warming effects than to increasing atmospheric N deposition (Figure 8).

Ocean warming and atmospheric N deposition both induce positive feedbacks on water column denitrification via the expansion of OMZs. However, the warming-driven reduction of exported organic matter at depth results in less N loss via reduced benthic denitrification. This compensating mechanism, together with declining N_2 fixation, counteract the increase in N deposition (Figure 8) and result in a small imbalance of $\sim$ +5 Tg N y^{-1} by the end of the 21st century. Over the centennial time scales considered in this study, this imbalance is much smaller than the hypothesized annual N loss exceeding 100 T g Ny^{-1} [*Codispoti et al.*, 2001; *Codispoti*, 2007] and is virtually indistinguishable from present-day uncertainty in the marine N balance [*Gruber*, 2004, 2008]. Despite the large expansion of OMZs, our model results suggest reduced subsurface N_2O production driven by shallower remineralization and reduced export production triggered by ocean warming. These processes, together with the slowdown of ocean circulation and increased atmospheric N_2O, contribute to lower future N_2O emissions.

While the current study does not incorporate all the feedbacks that may potentially impact on the N cycle (e.g., stoichiometric variability of phytoplankton, anthropogenically induced changes in ocean acidification and iron deposition), the results of our analysis suggest that numerous compensating mechanisms constrain

N inventory perturbations and that these mechanisms will help regulate marine productivity and oceanic N_2O emissions over the 21st century (Figure 8). Our results support the hypothesis that strong stabilizing feedbacks can explain the lack of variability of the N inventory across the Holocene [*Gruber*, 2004].

Acknowledgments
Work for this study was funded by Bundesministerium for Bildung und Forschung (BMBF) (SOPRAN grant FKZ 03F0662A; BIOACID grant FKZ 03F0728A) and Deutsche Forschungsgemeinschaft (DFG) (LA2919/1-1 and SFB754). Model data used in this study are available at https://thredds.geomar.de.

References

Arevalo-Martinez, D. L., A. Kock, C. R. Loscher, R. A. Schmitz, and H. W. Bange (2015), Massive nitrous oxide emissions from the tropical South Pacific Ocean, *Nat. Geosci.*, *8*(7), 530–533, doi:10.1038/ngeo2469.

Babbin, A. R., D. Bianchi, A. Jayakumar, and B. B. Ward (2015), Rapid nitrous oxide cycling in the suboxic ocean, *Science*, *348*, 1127–1129.

Bendtsen, J., K. M. Hilligsøe, J. L. S. Hansen, and L. Richardson (2015), Analysis of remineralisation, lability, temperature sensitivity and structural composition of organic matter from the upper ocean, *Prog. Oceanogr.*, *130*, 125–145, doi:10.1016/j.pocean.2014.10.009.

Bianchi, D., J. P. Dunne, J. L. Sarmiento, and E. D. Galbraith (2012), Data-based estimates of suboxia, denitrification, and N_2O production in the ocean and their sensitivities to dissolved N_2O, *Global Biogeochem. Cycles*, *26*, GB2009, doi:10.1029/2011GB004209.

Bohlen, L., A. W. Dale, and K. Wallmann (2012), Simple transfer functions for calculating benthic fixed nitrogen losses and C:N:P regeneration ratios in global biogeochemical models, *Global Biogeochem. Cycles*, *26*(3), GB3029, doi:10.1029/2011GB004198.

Bopp, L., et al. (2013), Multiple stressors of ocean ecosystems in the 21st century: Projections with CMIP5 models, *Biogeosciences*, *10*, 6225–6245, doi:10.5194/bg-10-6225-2013.

Breitbarth, E., A. Oschlies, and J. LaRoche (2007), Physiological constraints on the global distribution of Trichodesmium – Effect of temperature on diazotrophy, *Biogeosciences*, *4*, 53–61, doi:10.5194/bg-4-53-2007.

Cabre, A., I. Marinov, R. Bernardello, and D. Bianchi (2015), Oxygen minimum zones in the tropical Pacific across CMIP5 models: Mean state differences and climate change trends, *Biogeosciences*, *12*, 5429–5454, doi:10.5194/bg-12-5429-2015.

Cocco, V., et al. (2013), Oxygen and indicators of stress for marine life in multi-model global warming projections, *Biogeosciences*, *10*, 1849–1868, doi:10.5194/bg-10-1849-2013.

Codispoti, L. A. (2007), An oceanic fixed nitrogen sink exceeding 400 Tg N a^{-1} vs the concept of homeostasis in the fixed-nitrogen inventory, *Biogeosciences*, *4*(2), 233–253, doi:10.5194/bg-4-233-2007.

Codispoti, L. A., J. A. Brandes, J. P. Christensen, A. H. Devol, S. W. A. Naqvi, H. W. Paerl, and T. Yoshinari (2001), The oceanic fixed nitrogen and nitrous oxide budgets: Moving targets as we enter the anthropocene?, *Sci. Mar.*, *65*(S2), 85–105, doi:10.3989/scimar.2001.65s285.

de Jesus Mendes, P. A., and L. Thomsen (2012), Effects of ocean acidification on the ballast of surface aggregates sinking through the twilight zone, *PLoS ONE*, *7*(12), e50865, doi:10.1371/journal.pone.0050865.

DeVries, T., C. Deutsch, P. A. Rafter, and F. Primeau (2013), Marine denitrification rates determined from a global 3-D inverse model, *Biogeosciences*, *10*, 2481–2496, doi:10.5194/bg-10-2481-2013.

Dietze, H., and U. Löeptien (2013), Revisiting "nutrient trapping" in global coupled biogeochemical ocean circulation models, *Global Biogeochem. Cycles*, *27*(2), 265–284, doi:10.1002/gbc.20029.

Duce, R. A., et al. (2008), Impacts of atmospheric anthropogenic nitrogen on the open ocean, *Science*, *320*(5878), 893–897, doi:10.1126/science.1150369.

Dutkiewicz, S., B. A. Ward, J. R. Scott, and M. J. Follows (2013), Winners and losers: Phytoplankton habitat and productivity shifts in a warmer ocean, *Global Biogeochem. Cycles*, *26*, GB1012, doi:10.1002/gbc.20042.

Dutkiewicz, S., B. A. Ward, J. R. Scott, and M. J. Follows (2014), Understanding predicted shifts in diazotroph biogeography using resource competition theory, *Biogeosciences*, *11*, 5445–5461, doi:10.5194/bg-11-5445-2014.

Dutkiewicz, S., J. J. Morris, M. J. Follows, J. Scott, O. Levitan, S. T. Dyhrman, and I. Berman-Frank (2015), Impact of Ocean Acidification on the Structure of Future Phytoplankton Communities, *Nat. Clim. Change*, *5*, 1002–1006, doi:10.1038/nclimate2722.

Eppley, R. W. (1972), Temperature and phytoplankton growth in the sea, *Fishery Bull.*, *70*, 1063–1085.

Falkowski, P. G. (1997), Evolution of the nitrogen cycle and its influence on the biological sequestration of CO_2 in the ocean, *Nature*, *387*, 272–275.

Frame, C. H., and K. L. Casciotti (2010), Biogeochemical controls and isotopic signatures of nitrous oxide production by a marine ammonia-oxidizing bacterium, *Biogeosciences*, *7*(9), 2695–2709, doi:10.5194/bg-7-2695-2010.

Galbraith, E. D., A. Gnanadesikan, J. P. Dunne, and M. R. Hiscock (2010), Regional impacts of iron-light colimitation in a global biogeochemical model, *Biogeosciences*, *7*(3), 1043–1064.

Galbraith, E. D., M. Kienast, A. L. Albuquerque, M. A. Altabet, and F. Batista (2013), The acceleration of oceanic denitrification during deglacial warming, *Nat. Geosci.*, *6*(7), 579–584.

Galloway, J. N., et al. (2004), Nitrogen cycles: Past, present, and future, *Biogeochemistry*, *70*, 153–226, doi:10.1007/s10533-004-0370-0.

Gent, P. R., and J. C. McWilliams (1990), Isopycnal mixing in ocean circulation models, *J. Phys. Oceanogr.*, *20*(1), 150–155.

Getzlaff, J., and H. Dietze (2013), Effects of increased isopycnal diffusivity mimicking the unresolved equatorial intermediate current system in an Earth system climate model, *Geophys. Res. Lett.*, *40*, 2166–2170, doi:10.1002/grl.50419.

Getzlaff, J., H. Dietze, and A. Oschlies (2016), Effects of increased isopycnal diffusivity mimicking the unresolved equatorial intermediate current system in an Earth system climate model, *Geophys. Res. Lett.*, *43*, 728–734, doi:10.1002/2015GL066841.

Gillooly, J., J. Brown, G. West, and E. SavageVand Charnov (2001), Effects of size and temperature on metabolic rate, *Science*, *293*, 2248–2251.

Goreau, T. J., W. A. Kaplan, S. C. Wofsy, M. B. McElroy, F. W. Valois, and S. W. Watson (1980), Production of NO_2 and N_2O by nitrifying bacteria at reduced concentrations of oxygen, *Appl. Environ. Microbiol.*, *40*(3), 526–532.

Gruber, N. (2004), The dynamics of the marine nitrogen cycle and its influence on atmospheric CO_2, in *Carbon Climate Interactions*, edited by T. Oguz and M. Follows, pp. 97–148, Kluwer Acad., Dordrecht, Netherlands.

Gruber, N. (2008), The marine nitrogen cycle: Overview and challenges, in *Nitrogen in the Marine Environment, chap. 1*, edited by E. C. D. G. Capone, D. A. Bronk, and M. R. Mulholland, pp. 1–50, Elsevier, Amsterdam.

Gruber, N. (2016), Elusive marine nitrogen fixation, *Proc. Natl. Acad. Sci. U.S.A.*, *113*(16), 4246–4248, doi:10.1073/pnas.1603646113.

Hofmann, M., and H. Schellnhuber (2009), Oceanic acidification affects marine carbon pump and triggers extended marine oxygen holes, *Proc. Natl. Acad. Sci. U.S.A.*, *106*(9), 3017–3022.

Hutchins, D. A., F.-X. Fu, Y. Zhang, M. E. Warner, Y. Feng, K. Portune, P. W. Bernhardt, and M. R. Mulholland (2007), CO_2 control of Trichodesmium N_2 fixation, photosynthesis, growth rates, and elemental ratios: implications for past, present, and future ocean biogeochemistry, *Limnol. Oceanogr.*, *52*, 1293–1304, doi:10.4319/lo.2007.52.4.1293.

Ito, T., A. Nenes, M. S. Johnson, N. Meskhidze, and C. Deutsch (2016), Acceleration of oxygen decline in the tropical Pacific over the past decades by aerosol pollutants, *Nat. Geosci.*, *9*(6), 443–447.

Ji, Q., A. R. Babbin, A. Jayakumar, S. Oleynik, and B. B. Ward (2015), Nitrous oxide production by nitrification and denitrification in the Eastern Tropical South Pacific oxygen minimum zone, *Geophys. Res. Lett.*, *42*, 10,755–10,764, doi:10.1002/2015GL066853.

Jin, X., and N. Gruber (2003), Offsetting the radiative benefit of ocean iron fertilization by enhancing N_2O emissions, *Geophys. Res. Lett.*, *30*(24), 2249, doi:10.1029/2003GL018458.

Kalnay, E., et al. (1996), The NCEP/NCAR 40-year reanalysis project, *Bull. Am. Meteorol. Soc.*, *77*(3), 437–471, doi:10.1175/1520-0477(1996)0770437tnyrp2.0.co2.

Keller, D. P., A. Oschlies, and M. Eby (2012), A new marine ecosystem model for the University of Victoria Earth System Climate, *Model Geosci. Model Dev.*, *5*(5), 1195–1220.

Kim, I.-N., K. Lee, N. Gruber, D. M. Karl, J. L. Bullister, S. Yang, and T.-W. Kim (2014), Increasing anthropogenic nitrogen in the North Pacific Ocean, *Science*, *346*(6213), 1102–1106, doi:10.1126/science.1258396.

Klausmeier, C. A., E. Litchman, T. Daufresne, and S. A. Levin (2004), Optimal nitrogen-to-phosphorus stoichiometry of phytoplankton, *Nature*, *429*, 171–174, doi:10.1038/nature02454.

Kock, A., D. L. Arévalo-Martínez, C. R. Löscher, and H. W. Bange (2016), Extreme N_2O accumulation in the coastal oxygen minimum zone off Peru, *Biogeosciences*, *13*, 827–840, doi:10.5194/bg-13-827-2016.

Krishnamurthy, A., J. K. Moore, C. S. Zender, and C. Luo (2007), Effects of atmospheric inorganic nitrogen deposition on ocean biogeochemistry, *J. Geophys. Res.*, *112*, G02019, doi:10.1029/2006JG000334.

Krishnamurthy, A., J. K. Moore, N. Mahowald, C. Luo, S. C. Doney, K. Lindsay, and C. S. Zender (2009), Impacts of increasing anthropogenic soluble iron and nitrogen deposition on ocean biogeochemistry, *Global Biogeochem. Cycles*, *23*, GB3016, doi:10.1029/2008GB003440.

Krishnamurthy, A., J. K. Moore, N. Mahowald, C. Luo, and C. S. Zender (2010), Impacts of atmospheric nutrient inputs on marine biogeochemistry, *J. Geophys. Res.*, *115*, G01006, doi:10.1029/2009JG001115.

Kvale, K. F., K. J. Meissner, and D. P. Keller (2015), Potential increasing dominance of heterotrophy in the global ocean, *Environ. Res. Lett.*, *10*, doi:10.1088/1748-9326/10/7/074009.

Kwon, E. Y., F. Primeau, and J. L. Sarmiento (2009), The impact of remineralization depth on the air-sea carbon balance, *Nat. Geosci.*, *2*, 630–635, doi:10.1038/NGEO612.

Lamarque, J.-F., et al. (2013), Multi-model mean nitrogen and sulfur deposition from the Atmospheric Chemistry and Climate Model Intercomparison Project (ACCMIP): Evaluation of historical and projected future changes, *Atmos. Chem. Phys.*, *13*(16), 7997–8018, doi:10.5194/acp-13-7997-2013.

Landolfi, A., H. Dietze, W. Koeve, and A. Oschlies (2013), Overlooked runaway feedback in the marine nitrogen cycle: The vicious cycle, *Biogeosciences*, *10*(3), 1351–1363, doi:10.5194/bg-10-1351-2013.

Landolfi, A., W. Koeve, H. Dietze, P. Kähler, and A. Oschlies (2015), A new perspective on environmental controls of marine nitrogen fixation, *Geophys. Res. Lett.*, *42*, 4482–4489, doi:10.1002/2015GL063756.

Large, W. G., G. Danabasoglu, J. C. McWilliams, P. R. Gent, and F. O. Bryan (2001), Equatorial circulation of a global ocean climate model with anisotropic horizontal viscosity, *J. Phys. Oceanogr.*, *31*(2), 518–536.

Laufkötter, C., et al. (2015), Drivers and uncertainties of future global marine primary production in marine ecosystem models, *Biogeosciences*, *12*, 6955–6984, doi:10.5194/bg-12-6955-2015.

Laufkötter, C., et al. (2016), Projected decreases in future marine export production: The role of the carbon flux through the upper ocean ecosystem, *Biogeosciences*, *13*, 4023–4047, doi:10.5194/bg-13-4023-2016.

Löscher, C. R., A. Kock, M. Kšnneke, J. LaRoche, H. W. Bange, and R. A. Schmitz (2012), Production of oceanic nitrous oxide by ammonia-oxidizing archaea, *Biogeosciences*, *9*(7), 2419–2429, doi:10.5194/bg-9-2419-2012.

Mahowald, N. M., and C. Luo (2003), A less dusty future?, *Geophys. Res. Lett.*, *30*(17), 1903, doi:10.1029/2003GL017880.

Marsay, C. M., R. J. Sanders, S. A. Henson, K. Pabortsava, E. P. Achterberg, and R. S. Lampitt (2015), Attenuation of sinking particulate organic carbon flux through the mesopelagic ocean, *Proc. Natl Acad. Sci. U.S.A.*, *112*, 1089–1094.

Martinez-Rey, J., J. Bopp, M. Gehlen, A. Tagliabue, and N. Gruber (2015), Projections of oceanic N_2O emissions in the 21st century using the IPSL Earth system model, *Biogeosciences*, *12*, 4133–4148.

Martiny, A. C., C. T. A. Pham, F. W. Primeau, J. A. Vrugt, J. K. Moore, S. A. Levin, and M. W. Lomas (2013), Strong latitudinal patterns in the elemental ratios of marine plankton and organic matter, *Nat. Geosci.*, *6*(4), 279–283, doi:10.1038/ngeo1757.

Matsumoto, K. (2007), Biology-mediated temperature control on atmospheric pCO_2 and ocean biogeochemistry, *Geophys. Res. Lett.*, *34*, L20605, doi:10.1029/2007GL031301.

McMahon, K. W., M. D. McCarthy, O. A. Sherwood, T. Larsen, and T. P. Guilderson (2015), Millennial-scale plankton regime shifts in the subtropical North Pacific Ocean, *Science*, *350*, 1530, doi:10.1126/science.aad6946.

Meinshausen, M., et al. (2011), The RCP greenhouse gas concentrations and their extensions from 1765 to 2300, *Clim. Change*, *109*(1–2), 213–241, doi:10.1007/s10584-011-0156-z.

Mills, M. M., and K. R. Arrigo (2010), Magnitude of oceanic nitrogen fixation influenced by the nutrient uptake ratio of phytoplankton, *Nat. Geosci.*, *1*, 439–443, doi:10.1038/ngeo856.

Moisander, P., et al. (2010), Unicellular cyanobacterial distributions broaden the oceanic N_2 fixation domain, *Science*, *327*, 1512–1514, doi:10.1126/science.1185468.

Moore, C. M., et al. (2013), Processes and patterns of oceanic nutrient limitation, *Nat. Geosci.*, *6*, 701–710, doi:10.1038/ ngeo1765.

Moore, J. K., K. Lindsay, S. C. Doney, M. C. Long, and K. Misumi (2013), Marine ecosystem dynamics and biogeochemical cycling in the community Earth system model [CESM1(BGC)]: Comparison of the 1990s with the 2090s under the RCP4.5 and RCP8.5 scenarios, *J. Clim.*, *26*(23), 9291–9312, doi:10.1175/JCLI-D-12-00566.1.

Nevison, C., J. H. Butler, and J. W. Elkins (2003), Global distribution of N_2O and the N_2O-AOU yield in the subsurface ocean, *Global Biogeochem. Cycles*, *17*(4), 1119, doi:10.1029/2003GB002068.

Oschlies, A., K. G. Schulz, U. Riebesell, and A. Schmittner (2008), Simulated 21st centuryÕs increase in oceanic suboxia by CO_2-enhanced biotic carbon export, *Global Biogeochem. Cycles*, *22*, GB4008, doi:10.1029/2007GB003147.

Peltier, W. R. (2004), Global glacial isostacy and the surface of the ice-age Earth: The ICE-5G (VM2) model and GRACE, *Annu. Rev. Earth Planet. Sci.*, *32*(1), 111–149, doi:10.1146/annurev.earth.32.082503.144359.

Quigg, A., et al. (2003), The evolutionary inheritance of elemental stoichiometry in marine phytoplankton, *Nature*, *425*, 291–294.

Riebesell, U., et al. (2007), Enhanced biological carbon consumption in a high CO_2 ocean, *Nature*, *450*, 545–548.

Santoro, A. E., C. Buchwald, M. R. McIlvin, and K. L. Casciotti (2011), Isotopic signature of N_2O produced by Marine Ammonia-Oxidizing Archaea, *Science*, *333*, 1282–1285, doi:10.1126/science.1208239.

Schmidtko, S., L. Stramma, and M. Visbeck (2017), Decades of decline for oceanic oxygen, *Nature*, *542*, 335–339.

Schmittner, A., A. Oschlies, H. D. Matthews, and E. D. Galbraith (2008), Future changes in climate, ocean circulation, ecosystems and biogeochemical cycling simulated for a business-as-usual CO_2 emission scenario until 4000 AD, *Global Biogeochem. Cycles*, *22*, GB1013, doi:10.1029/2007GB002953.

Segschneider, J., and J. Bendtsen (2013), Temperature-dependent remineralization in a warming ocean increases surface pCO_2 through changes in marine ecosystem composition, *Global Biogeochem. Cycles*, *27*, 1214–1225, doi:10.1002/2013GB004684.

Simmons, H. L., S. R. Jayne, L. C. S. Laurent, and A. J. Weaver (2004), Tidally driven mixing in a numerical model of the ocean general circulation, *Ocean Model.*, *6*(3–4), 245–263.

Somes, C. J., and A. Oschlies (2015), On the influence of Ònon-RedfieldÓ dissolved organic nutrient dynamics on the spatial distribution of N_2 fixation and the size of the marine fixed nitrogen inventory, *Global Biogeochem. Cycles*, *29*, 973–993, doi:10.1002/2014GB005050.

Somes, C. J., A. Oschlies, and A. Schmittner (2013), Isotopic constraints on the pre-industrial oceanic nitrogen budget, *Biogeosciences*, *10*(9), 5889–5910, doi:10.5194/bg-10-5889-2013.

Somes, C. J., A. Landolfi, W. Koeve, and A. Oschlies (2016), Limited impact of atmospheric nitrogen deposition on marine productivity due to biogeochemical feedbacks in a global ocean model, *Geophys. Res. Lett.*, *43*, 4500–4509, doi:10.1002/2016GL068335.

Steinacher, M., et al. (2010), Projected 21st century decrease in marine productivity: A multi-model analysis, *Biogeosciences*, *7*, 979–1005, doi:10.5194/bg-7-979-2010.

Stramma, L., G. C. Johnson, J. Sprintall, and V. Mohrholz (2008), Expanding oxygen-minimum zones in the tropical oceans, *Science*, *320*, 655–658.

Stramma, L., A. Oschlies, and S. Schmidtko (2012), Mismatch between observed and modeled trends in dissolved upper-ocean oxygen over the last 50 yr, *Biogeosciences*, *9*(10), 4045–4057, doi:10.5194/bg-9-4045-2012.

Suntharalingam, P., J. L. Sarmiento, and J. R. Toggweiler (2000), Global significance of nitrous-oxide production and transport from oceanic low-oxygen zones — A modeling study, *Global Biogeochem. Cycles*, *14*(4), 1535–1370.

Suntharalingam, P, E. Buitenhuis, C. Le Quéré, F. Dentener, C. Nevison, J. H. Butler, H. W. Bange, and G. Forster (2012), Quantifying the impact of anthropogenic nitrogen deposition on oceanic nitrous oxide, *Geophys. Res. Lett.*, *39*, L07605, doi:10.1029/2011GL050778.

Tagliabue, A., et al. (2016), How well do global ocean biogeochemistry models simulate dissolved iron distributions?, *Global Biogeochem. Cycles*, *30*, 149–174, doi:10.1002/2015GB005289.

Taucher, J., and A. Oschlies (2011), Can we predict the direction of marine primary production change under global warming?, *Geophys. Res. Lett.*, *38*, L02603, doi:10.1029/2010GL045934.

Taucher, J., L. T. Bach, U. Riebesell, and A. Oschlies (2014), The viscosity effect on marine particle flux: A climate relevant feedback mechanism, *Global Biogeochem. Cycles*, *28*, 415–422, doi:10.1002/2013GB004728.

Trimmer, M., P.-M. Chronopoulou, S. T. Maanoja, R. C. Upstill-Goddard, V. Kitidis, and K. J. Purdy (2016), Nitrous oxide as a function of oxygen and archaeal gene abundance in the North Pacific, *Nat. Commun.*, *7*, 13451, doi:10.1038/ncomms13451.

Ward, B. B. (2013), Nitrification in Marine Systems, in *Nitrogen in the Marine Environment*, edited by D. G. Capone et al., pp. 199–261, Elsevier, Amsterdam.

Weber, T. S., and C. Deutsch (2012), Plankton diversity and ocean circulation regulate the ocean nitrogen reservoir, *Nature*, *489*, 419–422.

Weiss, R. F., and B. A. Price (1980), Nitrous oxide solubility in water and seawater, *Mar. Chem.*, *8*, 347–359.

Yang, S., and N. Gruber (2016), The anthropogenic perturbation of the marine nitrogen cycle by atmospheric deposition: Nitrogen cycle feedbacks and the 15N Haber-Bosch effect, *Global Biogeochem. Cycles*, *30*, 1418–1440, doi:10.1002/2016GB005421.

Yool, A., E. E. Popova, A. C. Coward, D. Bernie, and T. R. Anderson (2013), Climate change and ocean acidification impacts on lower trophic levels and the export of organic carbon to the deep ocean, *Biogeosciences*, *10*(9), 5831–5854, doi:10.5194/bg-10-5831-2013.

Zamora, L. M., and A. Oschlies (2014), Surface nitrification: A major uncertainty in marine N_2O emissions, *Geophys. Res. Lett.*, *41*, 4247–4253, doi:10.1002/2014GL060556.

Zamora, L. M., A. Oschlies, H. W. Bange, K. B. Huebert, J. D. Craig, A. Kock, and C. R. Löscher (2012), Nitrous oxide dynamics in low oxygen regions of the Pacific: Insights from the MEMENTO database, *Biogeosciences*, *9*(12), 5007–5022, doi:10.5194/bg-9-5007-2012.